Journal of Nuclear Medicine, published on April 28, 2022 as doi:10.2967/jnumed.122.263864

Development of Fluorinated NP-59: A Revival of Cholesterol Utilization Imaging with PET.

Allen F. Brooks†, Wade P. Winton†, Jenelle Stauff†, Janna Arteaga†, Bradford Henderson†, Jeremy Niedbala†, Peter J. H. Scott†‡, Benjamin L. Viglianti†*

†Division of Nuclear Medicine, Department of Radiology, The University of Michigan Medical School, Ann Arbor, Michigan 48109, United States

‡The Interdepartmental Program in Medicinal Chemistry, The University of Michigan, Ann Arbor, Michigan 48109, United States

*Corresponding Benjamin L. Viglianti
bviglia@med.umich.edu
University of Michigan Health System
Department of Radiology
NucMed B1G505
1500 E. Medical Center Drive
Ann Arbor, MI 48109-5030
734-615-1808

Allen F. Brooks
afb@umich.edu
University of Michigan Health System
Department of Radiology
NucMed B1G505
1500 E. Medical Center Drive
Ann Arbor, MI 48109-5030
734-615-1808

Running Title: Development of Fluorinated NP-59
Word Count: 4458

Abstract:
Background: Imaging of cholesterol utilization is possible with the iodine-131 scintiscanning/SPECT agent, NP-59. This agent provided a non-invasive measure of adrenal function and steroid synthesis. However, iodine isotopes resulted in poor resolution, manufacturing challenges, and high radiation dosimetry to patients that have limited their use and clinical impact. A fluorine-18 analogue would address these shortcomings while retaining the ability to image cholesterol utilization.
Purpose: The goal of this study was to prepare and evaluate a fluorine-18 analogue of NP-59 to serve as a PET imaging agent for functional imaging of the adrenal glands based on cholesterol use. Previous attempts to prepare such an analogue of NP-59 have proven elusive. Preclinical and clinical evaluation could be carried out once the new fluorine analogue of NP-59 production was established.
Method: The recent development of a new reagent for fluorination along with an improved route to the NP-59 precursor allowed for the preparation of a fluorine analogue of NP-59, FNP-59. The radiochemistry for the fluorine-18 radiolabeled ^{18}F-FNP-59 is described, rodent radiation dosimetry studies and in vivo imaging in New Zealand rabbits was carried out. After in vivo toxicity studies, an IND approval was obtained and the first in human images with dosimetry using the agent were acquired.
Results: In vivo toxicity studies demonstrated that FNP-59 is safe for use at intended dose. Biodistribution studies with ^{18}F-FNP-59 demonstrated a similar pharmacokinetic profile to NP-59, but with decreased radiation exposure. In vivo animal images demonstrate expected uptake in tissues that utilize cholesterol: gallbladder, liver, and adrenal glands. First in human images had no adverse events and demonstrated accumulation in target tissues (liver and adrenal glands). Manipulation of uptake was also demonstrated with patients that received cosyntropin, resulting in improved uptake.
Conclusion: ^{18}F-FNP-59 provided higher resolution images, with lower radiation dose to the subjects. It has the potential to provide a non-invasive test for patients with adrenocortical diseases.

Introduction:
Cholesterol is essential in numerous biological processes, and changes in the trafficking of cholesterol are an important feature of many diseases such as Cushing's syndrome, primary aldosteronism, hyperandrogenism, adrenocortical carcinoma, and most importantly based on number of patients affected, atherosclerosis. Given the importance of cholesterol, efforts to image its distribution and specifically its involvement in the adrenal glands was an area of focus. In the 1970's cholesterol analogues radiolabeled with iodine-131 were developed as scintiscanning agents, beginning with 19-iodocholesterol.[1] It was then discovered that a modification of the steroid scaffold via a thermal rearrangement gave NP-59, a remarkably improved tracer with superior adrenal uptake.[2] NP-59 was subsequently developed for the use of diagnosing primary aldosteronism and other related diseases of the adrenal cortex related to the increase utilization of cholesterol.

The precursor for aldosterone is cholesterol, and an excessive accumulation of cholesterol esters is present in primary aldosteronism which was exploited with imaging of NP-59 to differentiate bilateral adrenal gland hyperplasia versus a unilateral solitary adenoma when blood work indicated a hormone imbalance.[3-14] It has also been used to identify primary Cushing's disease and classify an adrenal lesion as adrenal cortical carcinoma when there is a lack of uptake.[2] NP-59 provided a non-invasive alternative to the gold standard for localizing abnormal cortical steroid production the invasive adrenal vein sampling (AVS) procedure. However, NP-59 never saw wide adoption as a diagnostic agent given iodine-131 limitations: 1) difficult synthesis, 2) requirement of a multiday imaging protocol allowing background tissue clearance, 3) free ^{131}Iodine accumulation in the thyroid 4) poor image quality due to high energy photon emitted by ^{131}I, and consequently 5) poor radiation dosimetry excluding its routine screening use. Although still used in Asia and Europe in select cases, production was discontinued at our institution the sole source in the United States. given improvements in CT/MRI coupled with NP-59's limitations. However, CT/MRI alone is unable to reliability differentiate bilateral adrenal gland hyperplasia versus a unilateral solitary adenoma in up to 50% of patients.[15,16] In the absence of NP-59, invasive adrenal vein sampling is the only method of determining lateralization of primary aldosteronism.

Given the limitations of NP-59, many efforts to image the cause of primary aldosteronism have been investigated that do not rely on cholesterol accumulation. These include metomidate labeled with ^{11}C or ^{18}F that relies on the detection of extra cortical adrenal tissue;[17] ^{18}F labeled ligands for CYP11B2, an enzyme involved with aldosterone production, which is overexpressed in functional adenomas;[18,19] and most recently CXCR-4 ligand analogues (notably ^{68}Ga- pentixafor), imaging over expression of the receptor in adrenal adenomas.[20-22] Imaging agents for these targets (CXCR-4 and CYP11B2) have the advantage of identifying adrenal adenomas based on the expression/overexpression of targets not generally seen in normal adrenal tissue, and likely have clinical utility for primary aldosteronism detection. However, as ligands they

have the limitation of not being a functional imaging agent. The signal observed from their imaging does not represent the production of aldosterone or the other steroid hormones produced by the adrenal gland. Consequently, imaging agents based on the precursor (cholesterol) of aldosterone (or other cortical steroid hormones) are able to represent their production by their uptake, similar to FDG as a surrogate of glycolysis. This allows cholesterol imaging to be used for primary aldosteronism; as well as, excessive cortisol production and other pathologies that rely on cholesterol.
In the years that followed NP-59's introduction and its study as an imaging agent for behavior as a labeled cholesterol, numerous efforts were undertaken in order to improve the molecule using various radionuclides and structural modifications, shown in Figure 1.[1,2,23-26] Prominent among these efforts was the preparation of a fluorine-18 analogue to yield an improved positron emission tomography (PET) imaging agent. However, those efforts over three decades failed to generate the fluorinated analogue.[23,24] Advances in fluorine chemistry and fluorine-18 radiochemistry now make the radiolabeling of a fluorinated cholesterol analogue (FNP-59) possible and demonstrated herein. This will provide higher resolution images with lower radioactive dose to the subject, and potentially offer a non-invasive alternative to AVS.

Material and Methods:

No potential conflicts of interest relevant to this article exist. All animal work was done under the approval by the IACUC at the University of Michigan. All human studies were performed under an FDA IND, registered at clinicaltrials.gov (NCT04532489 and NCT04546126), and local approval by the University of Michigan IRB with written informed consent obtained.

Synthesis of FNP-59 Reference Standard and ^{18}F-FNP-59:

The generation of a fluorinated analog of NP-59 has been attempted for more than 40 years.[24] Several advances in radiochemistry techniques have been developed by our lab that have allowed the development of FNP-59.[27,28] Before the synthesis of the radioactive version, a reference standard needed to be produced with nonradioactive fluoride. This reference standard would allow quality control to confirm the preparation of radioactive FNP-59 (^{18}F-FNP-59) and to perform toxicity studies for evaluation and IND approval of the agent for human study.

Preparation of the reference standard for FNP-59 was achieved and published by our group.[27] Once the non-radioactive FNP-59 standard was prepared, we turned our attention to ^{18}F-FNP-59. We were able to achieve the synthesis using the radiofluorination chemistry techniques pioneered at our facility over the past 5 years. Starting from cholesterol (Supplemental Figure 1), this synthesis requires fewer steps and utilized safer chemistry techniques than the synthesis of NP-59.[2] Specifically, the radiosynthesis utilizes only class 3 solvents (ICH Harmonization Guideline for residual solvents based on solvent toxicity), and is conducted according to current Good Manufacturing Practices, with the resulting dose formulated at a higher specific activity than NP-59.[28,29]

Detailed synthesis procedures including QC/HPLC data for the agent and intermediate precursors are provided in the supplemental section, or can be obtained upon request from the authors.

Preclinical Studies of ^{18}F-FNP-59:

Radiation Dosimetry: The ^{18}F-FNP-59 uptake and dosimetry studies were carried out in Sprague Dawley rats (n=4, 2m/2f) at 10, 30, 60, 120, and 360 minutes. Rats were anesthetized with isoflurane and ^{18}F-FNP-59 (3349 ± 827 kBq for 10 min; 3709 ± 255 kBq for 30 min; 3312 ± 608 kBq for 60 min; 3645 ± 71 kBq for 120 min; 8297 ± 237 kBq) was administered via tail vein injection. At the appropriate time points, animals were euthanized, and their tissues procured for measuring radioactivity. Radioactivity was measured in a well counter and expressed as decay-corrected percent of the injected dose per gram of tissue. This data was then compared to historical ^{131}I-NP-59 data as mean ± standard deviation. Radiation dosimetry was calculated from the distribution data and was used to determine estimates of human dosimetry with OLINDA/EXM 2.0 software.[29]

Toxicology Study: A single-dose acute toxicity study for FNP-59 was carried out at the Michigan State In Vivo Facility. In this study, male and female Sprague Dawley rats (n=20, 10M/10F) were administered 416 µg/kg FNP-59 intravenously, 1,000 times the expected human equivalent dose in the formulation to be used for PET imaging studies, and by the *i.v.* route to be used with ^{18}F-FNP-59. In the study, body weights were recorded; blood was collected at intervals for clinical chemistry and complete blood count; clinical observations were recorded daily; and food consumption was monitored. Two points (day 4 and day 15) were used for necropsies, with half of the males and females analyzed at each time point. Organs were inspected and weighed, and slides were prepared for pathology.

In-Vivo Imaging:

A pilot study was carried out with New Zealand rabbits. Rabbits (n=2) were anesthetized with isoflurane and were dosed via intravenous administration of ^{18}F-FNP-59 (2.26 ± 0.09 mCi). Imaging of the rabbits with PET (Concorde MicroPET) occurred at 2 and 3 hours. At 4 hours the rabbits were sacrificed and imaged on a clinical PET/CT scanner (Siemens Biograph True Point) within in 20 minutes of euthanasia.

Human Imaging:

With the above data, the Food and Drug Administration (FDA) has approved a physician-sponsored IND (#150397; PI, Benjamin L. Viglianti) in June 2020 to begin testing ^{18}F-FNP-59 in human subjects. A University of Michigan Institutional Review Board (IRB) protocol (#HUM00179097) is also approved. After informed consent, four subjects (>18 years, no known adrenal pathology, non-pregnant females) were chosen, 2 males and 2 females were imaged dynamically for 30 minutes following 6 mCi of ^{18}F-

FNP-59 injected into the antecubital fossa. Static imaging at a 3-hr time point (n=4) along with a 1-hr and 6-hr time point were also obtained (n=2 for each). An additional patient without adrenal pathology was imaged under adrenal stimulation to test if we could artificially increase uptake.

An additional 3 patients without adrenal pathology were imaged under adrenal stimulation to test if we could artificially increase ^{18}F-FNP-59 uptake. These patients were given 250 µg of cosyntropin intravenously over ~2 minutes. Five minutes after cosyntropin administration, 6 mCi of ^{18}F-FNP-59 was injected into the antecubital fossa. Dynamic imaging over the abdomen occurred for 30 minutes followed by a 1-hr and 3-hr whole body acquisition.

Human Radiation Dosimetry and Image Analysis:
Organs (liver, kidney, spleen, gallbladder, pancreas, kidneys, lungs, bones, heart, male gonads, and bladder) were segmented on MIM encore software and SUVs, absolute, and decay-corrected/attenuated counts were generated. Given the adrenal glands were non-enlarged, segmentation was not practical. Consequently a 2 cm sphere centered over the left adrenal gland was used for adrenal uptake measurement. The right adrenal gland was not directly measured to avoid partial volume effect from the liver. All counts measured from the left adrenal gland were doubled to account for this.

For each patient, measured uptake data was expressed as a percent of the injected dose in each organ. Time-activity curves were generated and the resulting fractions and half-times, or results of manual integrations were input into the OLINDA/EXM 2.0 software.[29,30] Radiation dose to each organ or tissue was then calculated using either the ICRP Adult Male or ICRP Adult Female models. All patients' results were then averaged and a 95% confidence interval for each organ was generated.

The segmentation used for radiation dosimetry was also used to report SUV versus time data. Results were reported as mean for the region of interest with a 95% confidence range.

Results:
Synthesis of FNP-59 Reference Standard and ^{18}F-FNP-59:
We have developed and demonstrated the synthesis of ^{18}F-FNP-59 starting from cholesterol. Final products and intermediates have been confirmed via NMR analysis and mass spectrometry. Precursor and reference standard purity (> 90%) were additionally confirmed via reverse phase HPLC using UV detection at 212 nm; detailed data for the synthesis and characterization is in the supplemental data for standard, precursor, and intermediates. The radiosynthesis utilizes only class 3 solvents, and is conducted according to current Good Manufacturing Practices, with the resulting dose formulated at a specific higher activity than those achieved for NP-59.[31,32]

Rodent Dosimetry: Biodistribution data in rats demonstrated increasing ^{18}F-FNP-59 adrenal and ovary uptake over time (Supplemental Figure 2A), as has been demonstrated to occur with ^{131}I-NP-59,[2] and is consistent with the expected trafficking of cholesterol. Importantly, the adrenal to liver ratio is greater than 5 to 1. This result overcomes one of the main limitations of ^{131}I-NP-59 imaging, the requirement of a multi-day imaging protocol to allow background uptake to dissipate to resolve the image. Additionally, the data demonstrated that imaging is possible within the decay time of ^{18}F (Supplemental Figure 2C).

Radiation dosimetry estimates were calculated based on both rodent and human biodistribution data (Table 1) using OLINDA/EXM 2.0 software. The results demonstrate a significantly decreased radiation dose in target organs (gonads/liver/adrenal/thyroid), compared with ^{131}I-NP-59 historical data as well as an overall effective dose that is nearly two orders of magnitude less than ^{131}I-NP-59 .[29]

In-vivo imaging results:
A pilot study in New Zealand rabbits was performed with PET images obtained at 1 and 4 hours. Subsequent PET/CT images taken immediately after euthanasia, shown in (Supplemental Figure 3). The results demonstrate expected ^{18}F-FNP-59 accumulation in the liver and the gallbladder. Gallbladder uptake was not seen in rats as they lack it anatomically, but had been seen in the historical NP-59 patients. More importantly, the rabbits demonstrated adrenal gland uptake in a similar temporal relationship to rat experiments but to a lesser degree, adrenal to liver ratio was ~2:1.

Human imaging results:
There were 4 humans (2M/2F) that were imaged with ^{18}F-FNP-59. In Supplemental Figure 4 is an example of a 20-year-old and in Figure 2 is a 21-year-old female imaged after 250 mcg cosyntropin injection. Both females had no known history of medical/endocrine disease and both imaged at 3 hours after injection of 6 mCi of ^{18}F-FNP-59. In all subjects there was intense tracer uptake in the liver and gallbladder, similar to the rabbit experiments (Figure 3). This uptake in the liver decreased with time as bile production occurred. Adrenal gland uptake was also seen, but was less than expected compared to the rat experiments. The adrenal to liver ratio was ~0.25:1 at 1 hour, ~0.5:1 at 3 hours, and ~1:1 at 6 hours for unstimulated subject (Figure 3C), compared to animal data that suggested at 5:1 ratio at 6 hours (Supplemental Figure 2). However, this adrenal to liver ratio did increase over time, following similar kinetics as to the rat experiments. Similarly, gonadal uptake (not shown) was less than the animal data had suggested it would have been.

Three subjects were pretreated with cosyntropin prior to ^{18}F-FNP-59 administration to stimulate adrenal gland cholesterol uptake through increased hormone synthesis (Figure 2). This resulted in more than doubling of ^{18}F-FNP-59 uptake at 1 and 3 hours (Figure 3B and C) along with increased uptake during dynamic phase imaging.

Overall, following injection of 40 ± 4 μg of ^{18}F-FNP-59, no adverse events were observed after injection or within the following days.

Discussion:
NP-59 has had a long and useful clinical history of identifying cholesterol utilization, accumulating in pathology where excessive production of hormones that use cholesterol as its backbone are produced. The most common use is for characterizing primary aldosteronism. Although its clinical utility has been established for the past ~40 years, limitations of the ^{131}I label allows it to only be used in select clinical cases, rather than broader screening applications given adverse dosimetry due to ^{131}I. It had been suggested that the tracer could be improved by replacing ^{131}I with ^{18}F (^{18}F-FNP-59), but the prior chemistry techniques attempted and described in the literature were unsuccessful.[23,24]

We have demonstrated an improved concise route to synthesize the FNP-59 reference standard and radiolabeling precursor. A GMP-compliant process has been developed for the production of ^{18}F-FNP-59 using only class three solvents in accordance with green radiochemistry principles.[33,34] In addition, radiation dosimetry calculations and single acute toxicity dosing studies have been conducted and showed the agent was safe and appropriate for the filing of an investigational new drug (IND) application to the FDA. The preliminary evaluation demonstrated that ^{18}F-FNP-59 behaved in a nearly identical manner to historical ^{131}I-NP-59 data, with a greatly improved safety profile given the two orders of magnitude reduction in radioactive dose to target organs, and that the required target to background ratios can be achieved within the physical half-life limitations of fluorine-18.

In vivo imaging was carried out in New Zealand rabbits. This animal model demonstrated ^{18}F-FNP-59 uptake in expected tissues (adrenal glands and liver). Notably, uptake was also seen in the gallbladder, which was expected and not seen in rats given their anatomical absence of a gallbladder.

First in human imaging for radiation dosimetry measurements was performed in four individuals. There were no serious adverse events, uptake in target organs observed, and the calculated radiation dose was nearly two orders of magnitude less than the historical ^{131}I-NP-59 radiation dose. Most importantly, uptake was observed in the adrenal glands, via functional imaging of cholesterol uptake. However, the adrenal to liver ratio was less than the animal biodistribution data would have suggested at ~1:1 (Figure 3C) rather then 5:1 (Supplemental Figure 2A) at 6 hours. Given the animal data, this ratio would likely continue to improve at later time points past 6 hours. However, given the physical half-life of ^{18}F (109.8 min), and the sensitivity of our current equipment coupled to partial volume effects that occur when imaging the small anatomy of a normal adrenal glands limits the ability of measuring the uptake past 6 hours.

If we could imagine at later time points, >6 hours, there would be more time available for the ^{18}F-FNP-59 (acting as free cholesterol) to be incorporated into lipoproteins (primarily HDL)[35-37] and then accumulate in the adrenal glands through scavenger receptors while the liver and gallbladder are cleared via excretion.[38] This process of cholesterol incorporation in to lipoproteins and subsequent redistribution occurs much quicker in rodents compared to humans[39] and is the result of improved adrenal to liver ratio seen in preclinical animal studies (Figure 3A). This difference with rodent vs humans' redistribution was the reason that the original ^{131}I-NP-59 agent was imaged 3 days after administration, which was possible given ^{131}I half-life.

Although ^{18}F-FNP-59 uptake in human adrenal glands was less than observed in rodents, the data here suggest that there may be enough activity to allow imaging at later time points than the 6 hours that was demonstrated. One of the purposed advantages of total-body PET/CT scanners coming on-line is that they offer greater sensitivity as more disintegrations are observed compared to standard equipment.[40,41] However, these advantages have yet to demonstrated, a future goal we are working toward.

Although we believe that delayed imaging may demonstrate improved adrenal uptake given the rates of biological redistribution of cholesterol, the need for delayed imaging may not be necessary when evaluating patients with pathology. Gross et al. showed that ~50% of normal ^{131}I-NP-59 uptake in dogs (which are more similar to humans than rats on how they handle cholesterol) was based on ACTH stimulated cortisol production, and 10-15% was aldosterone production.[42] In a situation where native/normal cortisol production is suppressed with dexamethasone, and a patient has pathologic primary aldosteronism, ^{18}F-FNP-59 uptake may be high enough to determine laterality of abnormal production. This manipulation maneuver, dexamethasone suppression of normal cortisol production, is needed with ^{131}I-NP-59 imaging to suppress normal cortisol production. When this is performed, very minimal adrenal uptake of ^{131}I-NP-59 is seen in a normal gland. A recent examination of ^{131}I-NP-59 uptake in primary adrenal aldosteronism from adenoma by Lu et al., describe the adrenal-to-liver ratio of ^{131}I-NP-59 as 2-2.8 following dexamethasone suppression depending on the genetic profile.[43] Similarly, there was a 40 to 75% increased uptake of ^{131}I-NP-59 in the pathologic adrenal gland versus the normal gland. Consequently, using Lu at al. data of uptake ratios and rearrangement, the average adrenal to liver ratio in a normal adrenal gland for ^{131}I-NP-59 would range from 1.1 to 1.6.

Stimulation with ACTH of 3 normal subjects demonstrated adrenal to liver ratio of at least ~1.2:1 at 3 hours, >2x the uptake in unstimulated subjects. If the uptake kinetics hold the adrenal to liver ratio at 6 hours would have been ~1.5-2:1. This degree of uptake is in the range of Lu et al. However, this data needs to be replicated with other normal subjects stimulated with cosyntropin and imaged at later time points. More

importantly testing in patients that have pathology with and without dexamethasone suppression needs to be performed.

Consequently, we are currently planning to image more patients at later time points, optimizing the imaging protocol along with imaging patients with and without dexamethasone and ACTH stimulation. This will give us the normal expected dynamic range of uptake that can be seen with this agent. Finally, we plan to study patients that have been diagnosed with primary aldosteronism and will receive adrenal vein sampling to determine if imaging by PET/CT using ^{18}F-FNP-59 can lateralize disease.

Overall this work demonstrates the initial feasibility of ^{18}F-FNP-59 to image cholesterol trafficking and specifically uptake in human cortical adrenal tissue. Future studies will explore if ^{18}F-FNP-59 can serve as a non-invasive method to imaging lateral versus bilateral cause of primary aldosteronism.

Acknowledgments:
Funding for this work is the result University of Michigan Department of Radiology, Fast Forward Medical Innovation (PI Viglianti), Michigan Memorial Phoenix Project (PI Viglianti), Michigan Drug Discovery (PI Brooks and Viglianti), and R01EB021155 (PI Scott).

KEY POINTS
QUESTION: Can a fluorinated NP-59 be made and successfully accumulate in the adrenal glands?

PERTINENT FINDINGS: Fluorinated NP-59 was made, demonstrate improved radiation dosimetry, and accumulated in the adrenal glands. This accumulation appears dependent on adrenal gland hormone synthesis similar to the prior iodine agent were overproduction/stimulation results in increased accumulation.

IMPLICATIONS FOR PATIENT CARE: With FNP-59 development we could now explore if this agent can identify the cause of primary aldosteronism (adenoma versus bilateral hyperplasia), potentially limiting the need for adrenal vein sampling prior to definitive therapy.

References

1. Counsell RE, Ranade VV, Blair RJ, Beierwaltes WH, Weinhold PA. Tumor localizing agents. IX. Radioiodinated cholesterol. *Steroids* 1970; **16**(3): 317-28.
2. Sarkar SD, Beierwaltes H, Ice RD, et al. A new and superior adrenal scanning agent, NP-59. *J Nucl Med* 1975; **16**(11): 1038-42.
3. Chen YC, Wei CK, Chen PF, Tzeng JE, Chuang TL, Wang Y-F. Seeking the invisible: I-131 NP-59 SPECT/CT for primary hyperaldosteronism. *Kidney international* 2009; **75**(6): 663-.
4. Chen Y-C, Chiu J-S, Wang Y-F. NP-59 SPECT/CT Imaging in Stage 1 Hypertensive and Atypical Primary Aldosteronism: A 5-Year Retrospective Analysis of Clinicolaboratory and Imaging Features. *The Scientific World Journal* 2013; **2013**: 317934-.
5. Chen Y-C, Su Y-C, Wei C-K, et al. Diagnostic value of I-131 NP-59 SPECT/CT scintigraphy in patients with subclinical or atypical features of primary aldosteronism. *Journal of biomedicine & biotechnology* 2011; **2011**: 209787-.
6. Kazerooni EA, Sisson JC, Shapiro B, et al. Diagnostic accuracy and pitfalls of [iodine-131]6-beta-iodomethyl-19-norcholesterol (NP-59) imaging. *J Nucl Med* 1990; **31**(4): 526-34.
7. Papierska L, Ćwikła J, Rabijewski M, Glinicki P, Otto M, Kasperlik-Załuska A. Adrenal (131)I-6β-iodomethylnorcholesterol scintigraphy in choosing the side for adrenalectomy in bilateral adrenal tumors with subclinical hypercortisolemia. *Abdominal Imaging* 2015; **40**(7): 2453-60.
8. White ML, Gauger PG, Doherty GM, et al. The role of radiologic studies in the evaluation and management of primary hyperaldosteronism. *Surgery* 2008; **144**(6): 926-33; discussion 33.
9. Wong KK, Komissarova M, Avram AM, Fig LM, Gross MD. Adrenal cortical imaging with I-131 NP-59 SPECT-CT. *Clin Nucl Med* 2010; **35**(11): 865-9.
10. Yen R-F, Wu V-C, Liu K-L, et al. 131I-6beta-iodomethyl-19-norcholesterol SPECT/CT for primary aldosteronism patients with inconclusive adrenal venous sampling and CT results. *Journal of nuclear medicine : official publication, Society of Nuclear Medicine* 2009; **50**(10): 1631-7.
11. Wong KK, Gandhi A, Viglianti BL, Fig LM, Rubello D, Gross MD. Endocrine radionuclide scintigraphy with fusion single photon emission computed tomography/computed tomography. *World J Radiol* 2016; **8**(6): 635-55.
12. Wale DJ, Wong KK, Viglianti BL, Rubello D, Gross MD. Contemporary imaging of incidentally discovered adrenal masses. *Biomedicine & Pharmacotherapy* 2017; **87**: 256-62.
13. Wu MH, Liu FH, Lin KJ, Sun JH, Chen ST. Diagnostic value of adrenal iodine-131 6-beta-iodomethyl-19-norcholesterol scintigraphy for primary aldosteronism: a retrospective study at a medical center in North Taiwan. *Nucl Med Commun* 2019; **40**(6): 568-75.
14. Wu VC, Hu YH, Er LK, et al. Case detection and diagnosis of primary aldosteronism - The consensus of Taiwan Society of Aldosteronism. *J Formos Med Assoc* 2017; **116**(12): 993-1005.
15. Nanba AT, Nanba K, Byrd JB, et al. Discordance between imaging and immunohistochemistry in unilateral primary aldosteronism. *Clin Endocrinol (Oxf)* 2017; **87**(6): 665-72.
16. Sam D, Kline GA, So B, Leung AA. Discordance Between Imaging and Adrenal Vein Sampling in Primary Aldosteronism Irrespective of Interpretation Criteria. *J Clin Endocrinol Metab* 2019; **104**(6): 1900-6.
17. Burton TJ, Mackenzie IS, Balan K, et al. Evaluation of the sensitivity and specificity of (11)C-metomidate positron emission tomography (PET)-CT for lateralizing aldosterone secretion by Conn's adenomas. *J Clin Endocrinol Metab* 2012; **97**(1): 100-9.
18. Abe T, Naruse M, Young WF, Jr., et al. A Novel CYP11B2-Specific Imaging Agent for Detection of Unilateral Subtypes of Primary Aldosteronism. *J Clin Endocrinol Metab* 2016; **101**(3): 1008-15.

19. Bongarzone S, Basagni F, Sementa T, et al. Development of [(18)F]FAMTO: A novel fluorine-18 labelled positron emission tomography (PET) radiotracer for imaging CYP11B1 and CYP11B2 enzymes in adrenal glands. *Nucl Med Biol* 2019; **68-69**: 14-21.
20. Ding J, Zhang Y, Wen J, et al. Imaging CXCR4 expression in patients with suspected primary hyperaldosteronism. *Eur J Nucl Med Mol Imaging* 2020; **47**(11): 2656-65.
21. Ding L, Li J, Wu C, Yan F, Li X, Zhang S. A self-assembled RNA-triple helix hydrogel drug delivery system targeting triple-negative breast cancer. *J Mater Chem B* 2020; **8**(16): 3527-33.
22. Heinze B, Fuss CT, Mulatero P, et al. Targeting CXCR4 (CXC Chemokine Receptor Type 4) for Molecular Imaging of Aldosterone-Producing Adenoma. *Hypertension* 2018; **71**(2): 317-25.
23. Kobayashi T, Maeda M, Haradahira T, Kojima M. Fluoro norcholesterol analogues. Synthesis of 6 beta-(2'-fluoro) ethyl-19-norcholest-5(10)-en-3 beta-ol. *Steroids* 1982; **39**(5): 585-93.
24. Kobayashi T, Maeda M, Komatsu H, Kojima M. Synthesis of 7-Fluoro-B-Homo-19-Norcholest-5(10)-En-3-Beta-Ol Acetate. *Chem Pharm Bull* 1982; **30**(9): 3082-7.
25. Kojima M, Maeda M, Komatsu H, et al. Radio-Bromine Labeled nor-Cholesterol Analogs - Synthesis and Tissue Distribution Study in Rats of Br-82 Labeled 6beta-Bromomethyl-19-Norcholest-5(10)-En-3beta-Ol. *Steroids* 1977; **29**(4): 443-51.
26. Riley A. THE DEVELOPMENT OF SELENIUM-75 CHOLESTEROL ANALOGUES. *Journal of Labelled Compounds* 1965; **207**(5002): 1134-5.
27. Winton WP, Brooks AF, Wong KK, Scott PJH, Viglianti BL. Synthesis of 6-(Fluoromethyl)-19-norcholest-5(10)-en-3-ol, a Fluorinated Analogue of NP-59, using the Mild Fluorinating Reagent, TBAF(Pinacol)(2). *Synopen* 2019; **3**(2): 55-8.
28. Winton WP, Viglianti BL, Wong KK, Scott PJ, Brooks AF. Improved Synthesis and Preclinical Evaluation of [18F]FNP-59: a Radiotracer for Imaging Cholesterol Trafficking. *Journal of Nuclear Medicine* 2020; **61**.
29. Stabin MG, Sparks RB, Crowe E. OLINDA/EXM: the second-generation personal computer software for internal dose assessment in nuclear medicine. *J Nucl Med* 2005; **46**(6): 1023-7.
30. Stabin MG, Siegel JA. Physical models and dose factors for use in internal dose assessment. *Health Phys* 2003; **85**(3): 294-310.
31. Branch SK. Guidelines from the International Conference on Harmonisation (ICH). *J Pharm Biomed Anal* 2005; **38**(5): 798-805.
32. Wang T, Jacobson-Kram D, Pilaro AM, et al. ICH guidelines: inception, revision, and implications for drug development. *Toxicol Sci* 2010; **118**(2): 356-67.
33. Shao X, Fawaz MV, Jang K, Scott PJ. Ethanolic carbon-11 chemistry: the introduction of green radiochemistry. *Appl Radiat Isot* 2014; **89**: 125-9.
34. Stewart MN, Hockley BG, Scott PJ. Green approaches to late-stage fluorination: radiosyntheses of (18)F-labelled radiopharmaceuticals in ethanol and water. *Chem Commun (Camb)* 2015; **51**(79): 14805-8.
35. Schwartz CC, Berman M, Vlahcevic ZR, Halloran LG, Gregory DH, Swell L. Multicompartmental analysis of cholesterol metabolism in man. Characterization of the hepatic bile acid and biliary cholesterol precursor sites. *J Clin Invest* 1978; **61**(2): 408-23.
36. Schwartz CC, Berman M, Vlahcevic ZR, Swell L. Multicompartmental analysis of cholesterol metabolism in man. Quantitative kinetic evaluation of precursor sources and turnover of high density lipoprotein cholesterol esters. *J Clin Invest* 1982; **70**(4): 863-76.
37. Schwartz CC, Vlahcevic ZR, Berman M, Meadows JG, Nisman RM, Swell L. Central role of high density lipoprotein in plasma free cholesterol metabolism. *J Clin Invest* 1982; **70**(1): 105-16.
38. Kraemer FB. Adrenal cholesterol utilization. *Mol Cell Endocrinol* 2007; **265-266**: 42-5.

39. Bravo E, Botham KM, Mindham MA, Mayes PA, Marinelli T, Cantafora A. Evaluation in vivo of the differential uptake and processing of high-density lipoprotein unesterified cholesterol and cholesteryl ester in the rat. *Biochim Biophys Acta* 1994; **1215**(1-2): 93-102.
40. Vandenberghe S, Moskal P, Karp JS. State of the art in total body PET. *EJNMMI Phys* 2020; **7**(1): 35.
41. Badawi RD, Shi H, Hu P, et al. First Human Imaging Studies with the EXPLORER Total-Body PET Scanner. *J Nucl Med* 2019; **60**(3): 299-303.
42. Gross MD, Grekin RJ, Brown LE, Marsh DD, Beierwaltes WH. The relationship of adrenal iodocholesterol uptake to adrenal zona glomerulosa function. *J Clin Endocrinol Metab* 1981; **52**(4): 612-5.
43. Lu CC, Yen RF, Peng KY, et al. NP-59 Adrenal Scintigraphy as an Imaging Biomarker to Predict KCNJ5 Mutation in Primary Aldosteronism Patients. *Front Endocrinol (Lausanne)* 2021; **12**: 644927.

^{18}F-FNP59	Human Gender Average Dose		Rodent Gender Average Dose	Human ^{131}I-NP59* Average Dose	FDG** Average Dose
Target Organ	(mSv/MBq)	±95% error (mSv/MBq)	(mSv/MBq)	(mSv/MBq)	(mSv/MBq)
Adrenals	2.72E-02	6.82E-03	6.82E-02	4.0E+00	1.3E-02
Brain	7.92E-03	1.41E-03	3.70E-03		1.9E-02
Breasts	8.43E-03	1.12E-02	1.17E-02	4.0E-01	9.2E-03
Esophagus	1.43E-02	1.90E-03	1.43E-02		
Eyes	7.94E-03	1.42E-03	5.22E-03		
Gallbladder Wall	3.09E-01	3.73E-01	2.11E-02		1.3E-02
Left colon	1.40E-02	3.91E-03	2.85E-02		
Small Intestine	1.34E-02	3.71E-03	5.14E-02	4.1E-01	1.3E-02
Stomach Wall	1.48E-02	3.18E-03	1.57E-02	4.0E-01	1.3E-02
Right colon	1.88E-02	9.58E-03	5.76E-02		
Rectum	1.07E-02	2.09E-03	1.65E-02		
Heart Wall	1.10E-02	3.02E-03	1.60E-02		5.9E-02
Kidneys	1.91E-02	9.46E-03	1.51E-02	4.1E-01	2.0E-02
Liver	7.29E-02	7.70E-03	3.45E-02	1.2E+00	1.6E-02
Lungs	2.19E-02	8.57E-03	2.44E-02		1.7E-02
Ovaries	1.06E-02	1.72E-02	3.11E-02	3.8E-01	1.4E-02
Pancreas	1.91E-02	1.01E-02	1.68E-02	4.3E-01	2.6E-02
Prostate	1.69E-02	1.08E-02	1.32E-02		
Salivary Glands	8.90E-03	1.95E-03	1.10E-02		
Red Marrow	1.07E-02	2.14E-03	1.22E-02	3.9E-01	1.3E-02
Osteogenic Cells	1.66E-02	5.59E-03	1.04E-02	3.7E-01	
Spleen	5.75E-02	7.92E-02	3.36E-02	3.9E-01	3.8E-02
Testes	9.99E-03	2.94E-02	6.02E-03	3.6E-01	1.1E-02
Thymus	1.16E-02	2.16E-03	1.40E-02		1.2E-02
Thyroid	1.01E-02	2.38E-03	1.25E-02	3.0E+01	1.1E-02
Urinary Bladder Wall	1.11E-02	5.23E-03	1.32E-02	3.9E-01	8.6E-02
Uterus	1.03E-02	1.63E-02	1.54E-02	4.0E-01	1.7E-02
Total Body	1.20E-02	2.08E-03	1.36E-02		
Effective Dose:	1.75E-02	5.33E-03	1.92E-02	5.6E+01	

* ICRP 53

** FDA product Insert

Table 1: Human dosimetry mSv/mCi injected of [^{18}F]FNP-59 (n=4, 2M/2F). Rodent derived human estimated ^{18}F-FNP-59, Human ^{131}I-NP-59, and human ^{18}F-FDG dosimetry is shown for comparison. Significant decreased dose, 2 orders of magnitude, is seen with ^{18}F-FNP-59 compared to ^{131}I-NP-59. *published data ** FDA product insert

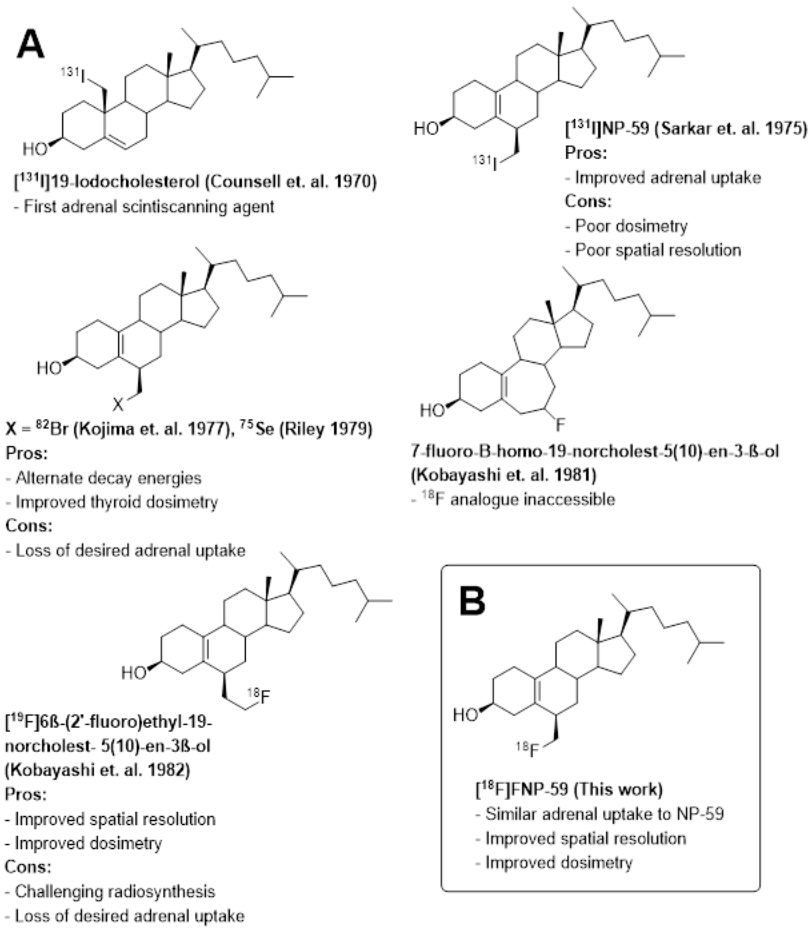

Figure 1: (A) Examples of previous efforts to prepare cholesterol based adrenal imaging agents and their limitations. (B) The improved adrenal imaging agent ^{18}F-FNP-59 and its advantages.

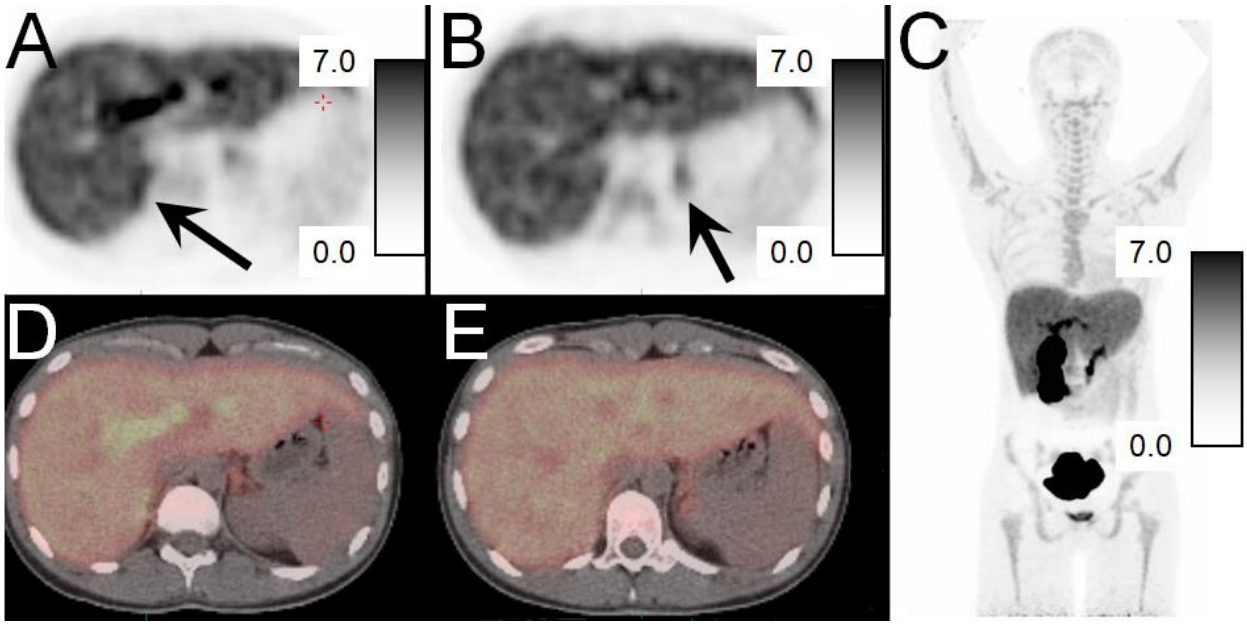

Figure 2: PET/CT images of ^{18}F-FNP-59 in a 21-year-old female without adrenal pathology and pretreated with cosyntropin given prior to 6 mCi of ^{18}F-FNP-59. Axial PET images obtained 3 hours after injection of the upper abdomen with adrenal glands (black arrows) identified on the right (A) and left (B). Scale bars are 0-7 SUV. Adrenal to liver ratio at ~1.3:1 on the right and 1:1.1 on the left at 3 hours. Fused PET/CT images of the adrenal glands are also shown (D,E) along with maximum intensity pixel image (C) that demonstrates expected gallbladder/biliary/bowel uptake given bile secretion.

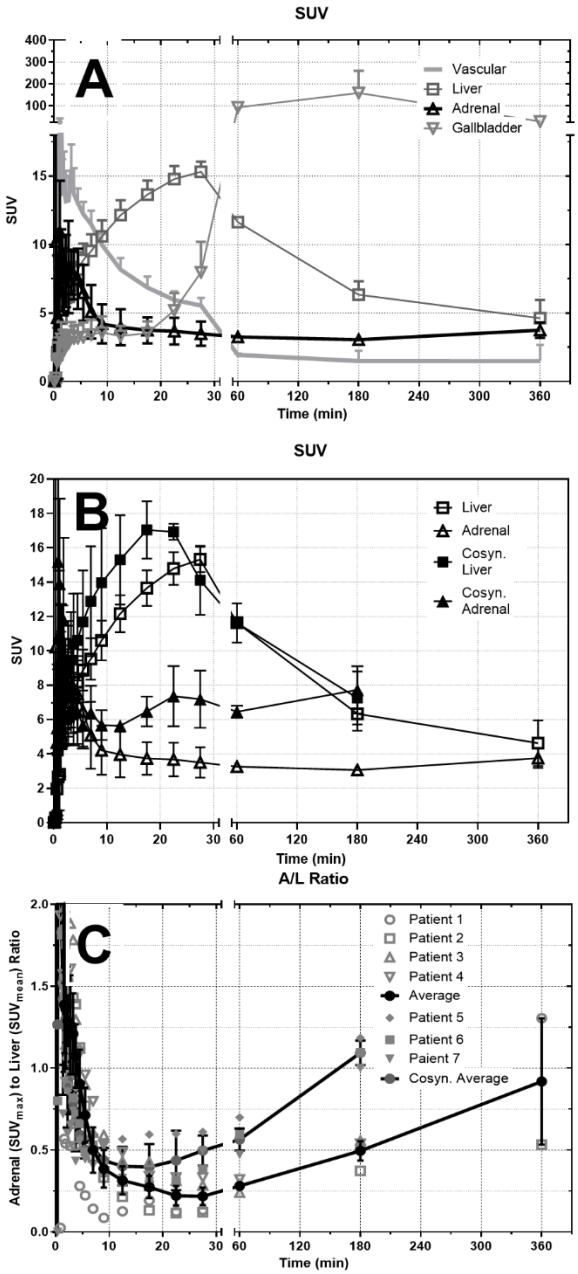

Figure 3: SUV ^{18}F-FNP-59 uptake in selected organ versus time in nonstimulated patients (n = 4;2M/2F at 180 min, n = 2 at 60 and 360 minutes) (A). Over time, after first pass, liver uptake slowly clears as ^{18}F-FNP-59 is excreted into bile and sent back out into the entero-hepatic circulation. Uptake comparison in the liver and adrenal gland of three patients stimulated with cosyntropin showing significant increased uptake in the adrenal gland (B) Overtime, left adrenal uptake slowly increases. The adrenal to liver ratio is also shown (C), demonstrating increasing ratio overtime after first pass vascular uptake (time < 30 minutes) is cleared. Additionally, the adrenal to liver ratio of three female patients (#5-7) given cosyntropin is shown. This resulted in significant increased uptake ratio compared to the unstimulated patients. Error bars are SEM.

Note, n = 4 for dynamic imaging and at 180 min, n = 2 at 60 and 360 minutes for patients #1-4.

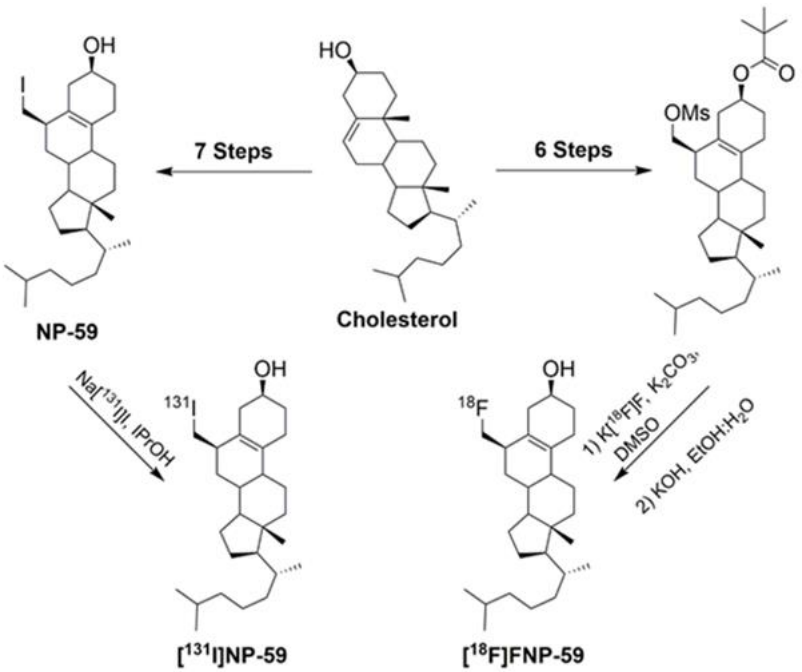

Supplemental Figure 1: Synthesis of ^{18}F-FNP-59 and ^{131}I-NP-59 from cholesterol. Note identical structure other than a fluorine substitution for iodine.

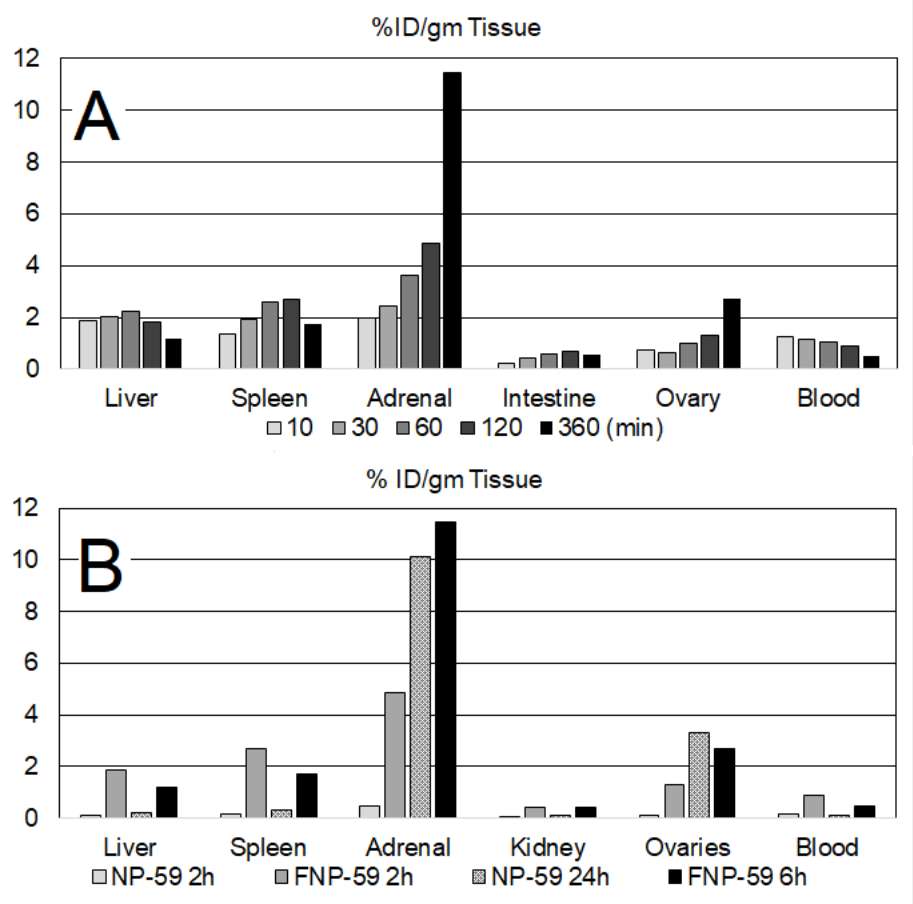

Supplemental Figure 2: Mean ^{18}F-FNP-59 uptake %injected dose per gm tissue (n=4) in rats **(A)** is shown. There is significant expected accumulation in the adrenal glands. Comparison to published mean ^{131}I-NP-59 human uptake is shown **(B)** indicating similar uptake within the decay time of ^{18}F.

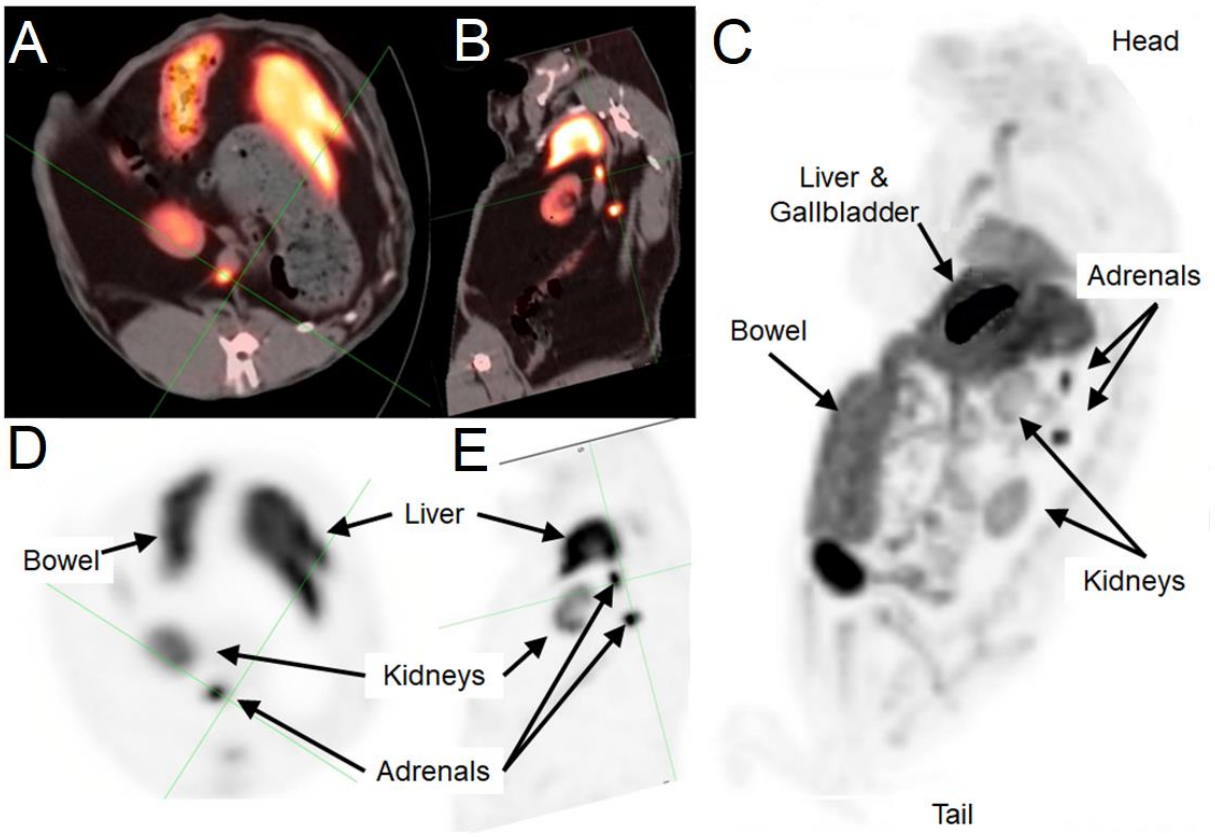

Supplemental Figure 3: Oblique axial (A, D) and oblique coronal images (B, E) of a rabbit given FNP-59 4 hours prior. Fused PET/CT (A, B) and PET (D, E) images are shown along with a MIP image (C). The adrenal glands are clearly visible along with expected uptake in the liver and accumulation in the gallbladder.

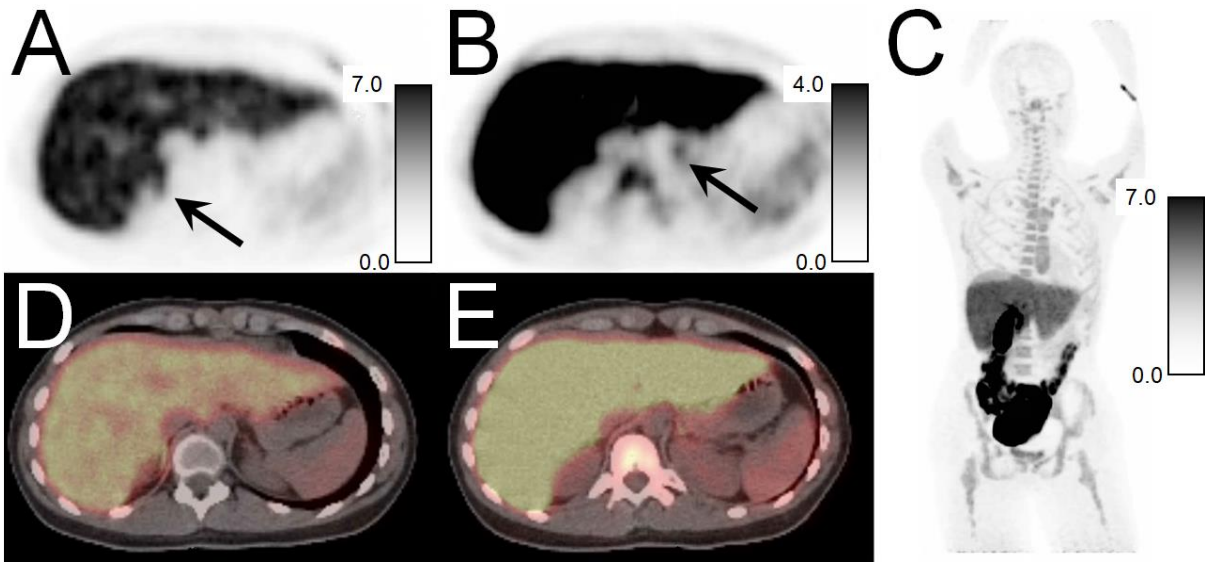

Supplemental Figure 4: PET/CT images of ^{18}F-FNP-59 in a 20-year-old female without adrenal pathology. Images were acquired 3hrs after injection of 6 mCi of ^{18}F-FNP-59. Axial PET images of the upper abdomen with adrenal glands (black arrows) identified on the right (A) and left (B). Scale bars are 0-7 SUV and 0-4 SUV respectively. Adrenal to liver ratio at ~1:1 on the left and 0.5:1 on the right. Fused PET/CT images of the adrenal glands are also shown (D, E) along with maximum intensity pixel image (C) also demonstrated expected gallbladder/biliary/bowel uptake given bile secretion.

Development of Flourinated NP-59: A Revival of Cholesterol Utilization Imaging with PET

Allen F. Brooks†, Wade P. Winton†, Jenelle Stauff†, Janna Arteaga†, Bradford Henderson†, Jeremy Niedbala†, Peter J. H. Scott†‡, Benjamin L. Viglianti†#*

†Division of Nuclear Medicine, Department of Radiology, The University of Michigan Medical School, Ann Arbor, Michigan 48109, United States

‡The Interdepartmental Program in Medicinal Chemistry, The University of Michigan, Ann Arbor, Michigan 48109, United States

#Nuclear Medicine Service, Ann Arbor Veterans Administration, 2215 Fuller Rd, Ann Arbor, Michigan, 48105, United States

*Corresponding bviglia@med.umich.edu

Table of Contents

1. Chemistry and Characterization…….....2
   1.1. General Considerations
   1.2. Synthesis of FNP-59 Reference Standard
   1.3. Synthesis of [^{18}F]FNP-59 Precursor

2. Radiochemistry……...6
   2.1. General Considerations.
   2.2. Radiochemical Synthesis of [^{18}F]FNP-59
   2.3. Manufacturing Flow Diagram
   2.4. Representative Batch Data
   2.5. HPLC and TLC Data

3. Biodistribution and Dosimetry Study…...…….……..15
   3.1 Biodistribution Study
   3.2 Human Radiation **Dosimetry** Estimates

4. Single Dose Acute Toxicity Study….……..17
   4.1. General Considerations
   4.2. Study Conducted

5. References……...18

6. ^{1}H NMR, ^{13}C NMR and HRMS Spectra…….18

1. Chemistry and Characterization

1.1. General Considerations

All the chemicals were purchased from commercially available suppliers and used without purification. Automated flash chromatography was performed with Biotage Isolera Prime system. High-performance liquid chromatography (HPLC) was performed using a Shimadzu LC-2010A HT system equipped with a Bioscan B-FC-1000 radiation detector. ^{1}H and ^{13}C NMR spectra: Varian 400 apparatus (400 MHz for ^{1}H NMR and 101 MHz for ^{13}C NMR), in $CDCl_3$ unless otherwise indicated, δ in ppm rel. to tetramethylsilane (δ = 0), J in Hz. Mass spectra were measured on an Agilent Q-TOF HPLC-MS or VG (Micromass) 70-250-S Magnetic sector mass spectrometer employing the electrospray ionization (ESI) method.

1.2. Synthesis of FNP-59 Reference Standard

Reference standard was prepared as previously described.[1]

1.3. Synthesis of FNP-59 Precursor

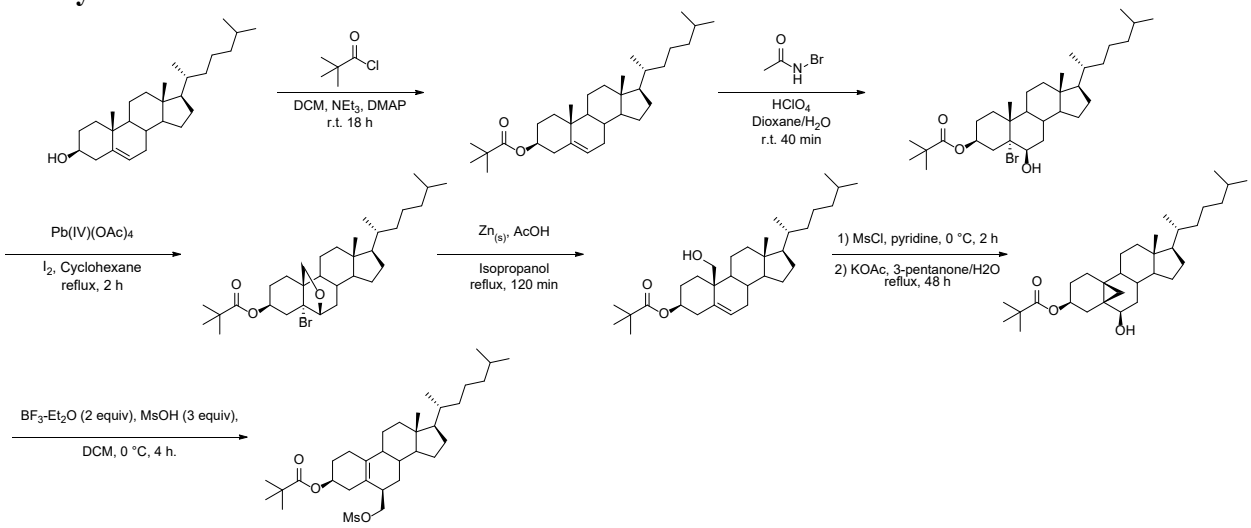

Figure S2: Synthesis of precursor for FNP-59 from cholesterol.

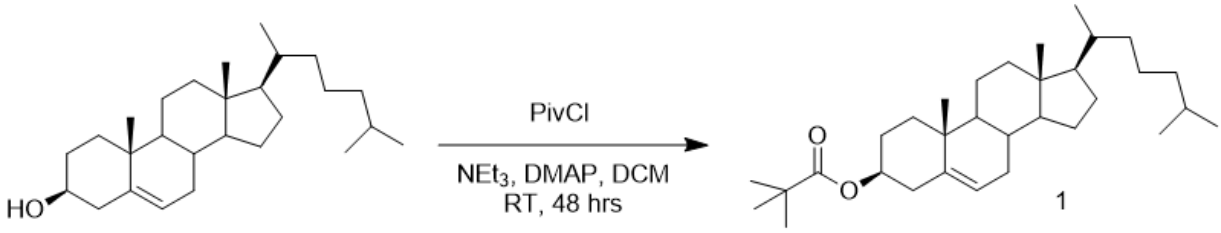

(3S,10R,13R,17R)-10,13-dimethyl-17-((R)-6-methylheptan-2-yl)-2,3,4,7,8,9,10,11,12,13,14,15,16,17-tetradecahydro-1H-cyclopenta[a]phenanthren-3-yl pivalate (Cholest-5-en-3-pivaloate) 1. As seen in figure 1, the synthesis begins with cholesterol. Cholesterol (10 g, 25.86 mmol) was added to a flame dried flask and dissolved in dichloromethane (50 mL). To this solution, triethylamine (4.32 mL, 31.03 mmol) and dimethylaminopyridine (0.3164 g, 2.59 mmol) were added. The solution was then cooled to 0°C, and pivaloyl chloride (3.5 mL, 28.45 mmol) was added dropwise while stirring. The reaction was then stirred at room temperature for 48 hours. The solvent was removed in vacuo, and the residue was triturated in 75 mL of hot acetone for 10 minutes, and then 5 mL of water was added. The suspension was allowed

to cool for 2 hours, and then the liquid was removed by vacuum filtration to give **1** as a white powder (10.8628 g, 89.2%) **TLC** R_F = 0.86, 1:9 EtOAc:Hexane. **^{1}H-NMR** (400.53 MHz, $CDCl_3$): δ 5.36 (1H, d, J = 4.62 Hz, 6-H), 4.56 (1H, m, 3α-H), 1.18 (9H, s, 3β-OPiv). **^{13}C-NMR** (100.13 MHz, $CDCl_3$): δ 177.98, 139.77, 122.46, 73.52, 56.67, 56.11, 49.99, 42.30, 39.72, 39.50, 38.59, 38.00, 36.97, 36.60, 36.17, 35.79, 31.88, 28.22, 28.00, 27.65, 27.15, 24.28, 23.82, 22.81, 22.56, 21.03, 19.36, 18.71, 11.84. **HR-MS** (ESI+) $[M+NH_4]^+$ Calculated for $C_{32}H_{54}O_2$: 488.4462; Found: 488.4460.

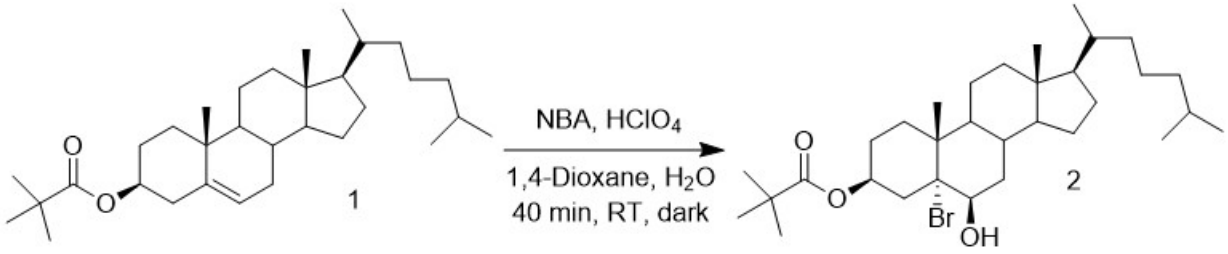

(3S,5R,6R,10R,13R,17R)-5-bromo-6-hydroxy-10,13-dimethyl-17-((R)-6-methylheptan-2-yl)hexadecahydro-1H-cyclopenta[a]phenanthren-3-yl pivalate (5-Bromocholestan-6-hydroxy-3-pivaloate) 2. Compound **1** (5 g, 10.62 mmol) was dissolved in dioxane (50 mL). A solution of perchloric acid (6.37 mL of 0.5M) was added while stirring. The reaction vessel was then wrapped in foil, and N-bromoacetamide (2.2708 g, 16.46 mmol) was added slowly over 5 minutes. The reaction was stirred for 40 minutes before being quenched by the addition of 10% sodium thiosulfate solution (50 mL). The mixture was then extracted with diethyl ether 3 times, and the resulting organic layer was isolated and dried over sodium sulfate. The solvent was removed in vacuo, and the material was purified by flash chromatography (20 g silica, 1:19 EtOAc:Hexane) yielding **2** as an off-white solid (2.8562 g, 47.4%). **TLC** R_F = 0.42, 1:9 EtOAc:Hexane. **^{1}H-NMR** (400.53 MHz, $CDCl_3$): δ 5.44 (1H, m, 3α-H), 4.19 (1H, s, 6β-OH), 2.47 (1H, m, 6α-H), 1.18 (9H, s, 3β-OPiv). **^{13}C-NMR** (100.13 MHz, $CDCl_3$): δ 177.98, 86.82, 75.79, 71.78, 56.07, 55.70, 47.42, 42.68, 40.36, 39.65, 39.49, 38.61, 38.31, 36.11, 35.75, 35.12, 34.59, 30.57, 28.19, 28.00, 27.16, 26.23, 24.05, 23.79, 22.81, 22.55, 21.31, 18.67, 18.08, 12.19. **HR-MS** (ESI+) $[M+NH_4]^+$ Calculated for $C_{32}H_{55}BrO_3$: 584.3673; Found: 584.3663.

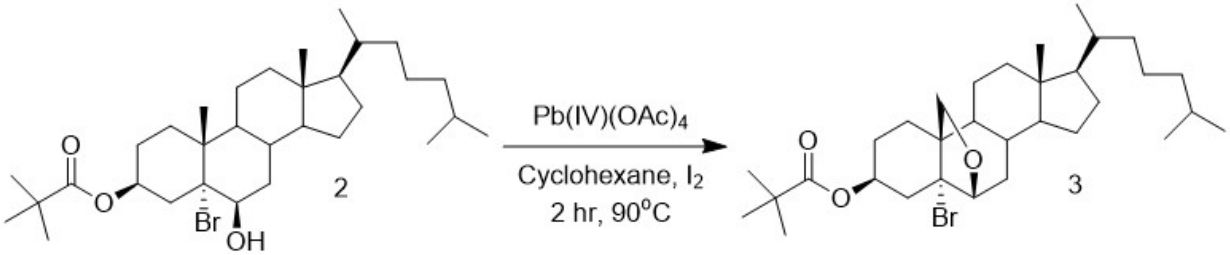

(3S,5R,6R,10R,13R,17R)-5-bromo-13-methyl-17-((R)-6-methylheptan-2-yl)hexadecahydro-6,10-(epoxymethano)cyclopenta[a]phenanthren-3-yl pivalate (5-Bromocholestan-6(19)-oxo-3-pivaloate) 3. Compound **2** (2.88562 g, 5.031 mmol) was added to a flame dried flask and dissolved in cyclohexane (50 mL). To this solution, lead tetraacetate (2.7884 g, 6.289 mmol) and iodine (0.6386 g, 2.516 mmol) were added while stirring. The reaction was then stirred at 90°C for 2 hours. It was then allowed to cool to room temperature, and then filtered. The filter was then washed with diethyl ether. The filtrate was then partitioned with a 10% solution of sodium thiosulfate, and the mixture was extracted with additional diethyl ether. The organic layer was then

washed with water and brine. The solvent was removed in vacuo to give **3** as a white solid (2.5381 g, 89.1%). **TLC** R_F = 0.69, 1:9 EtOAc:Hexane. Used directly in following step.

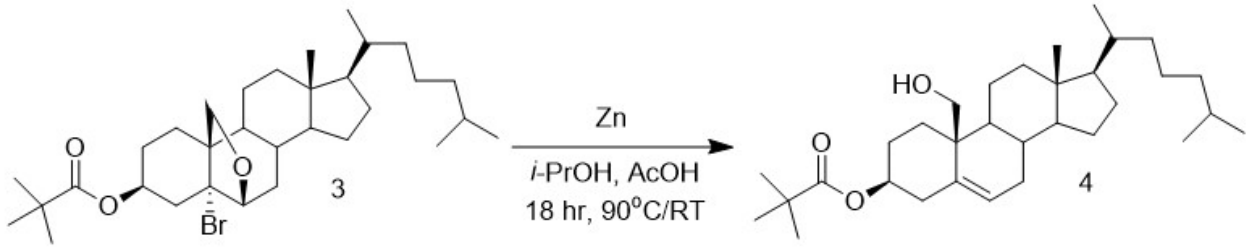

(3S,10S,13R,17R)-10-(hydroxymethyl)-13-methyl-17-((R)-6-methylheptan-2-yl)-2,3,4,7,8,9,10,11,12,13,14,15,16,17-tetradecahydro-1H-cyclopenta[a]phenanthren-3-yl pivalate (Cholest-5-en-19-hydroxy-3-pivaloate) 4. Compound **3** (2.5381 g, 4.48 mmol) was dissolved in isopropanol (45 mL) and glacial acetic acid (2.6 mL). Zinc powder was activated by being stirred under vacuum at 80 °C. The activated zinc (1.6125 g, 24.66 mmol) was then added while stirring. The reaction was then stirred at 90°C for 30 minutes, before being removed from heat, and allowed to stir at room temperature for an additional 18 hours. The resulting mixture was allowed to settle, and the liquid was decanted off. The solid was then decanted 3 more times with dichloromethane. The solvent was removed in vacuo and the material was purified by flash chromatography (20 g silica, 1:19 EtOAc:Hexane) to give **4** as a white solid (0.6970 g, 31.9%). **TLC** R_F = 0.28, 1:9 EtOAc:Hexane. **^{1}H-NMR** (400.53 MHz, $CDCl_3$): δ 5.76 (1H, d, J = 4.15 Hz, 6-H), 4.61 (1H, m, 3α-H), 3.85 (1H, d, J = 11.28 Hz, 19-H), 3.63 (1H, t, J = 9.17 Hz, 19-H), 1.17 (9H, s, 3β-OPiv). **^{13}C-NMR** (100.13 MHz, $CDCl_3$): δ 177.94, 134.66, 128.10, 72.96, 62.68, 57.53, 56.08, 50.25, 42.50, 41.60, 39.99, 39.49, 38.59, 38.08, 36.15, 35.77, 33.34, 33.02, 31.26, 28.23, 27.99, 27.12, 24.08, 23.82, 22.82, 22.56, 21.77, 18.69, 12.19. **HR-MS** (ESI+) $[M+H]^+$ Calculated for $C_{32}H_{54}O_3$: 487.4146; Found: 487.4140. $[M+NH_4]^+$ Calculated for $C_{32}H_{54}O_3$: 504.4411; Found: 504.4412. $[M+Na]^+$ Calculated for $C_{32}H_{54}O_3$: 509.3965; Found: 509.3963.

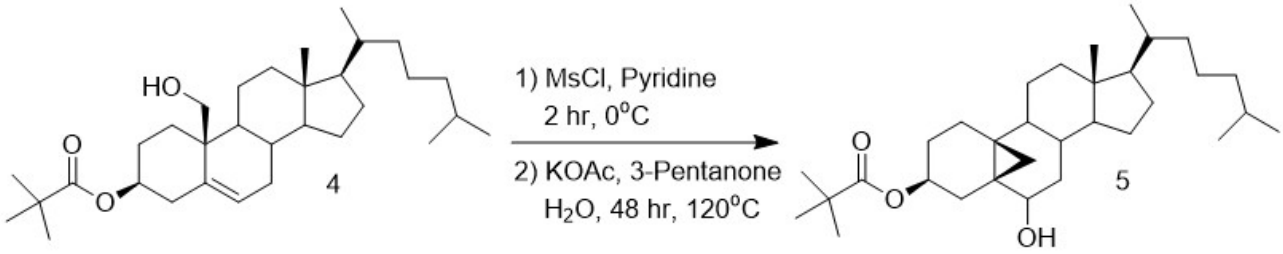

(3S,5R,10S,13R,17R)-6-hydroxy-13-methyl-17-((R)-6-methylheptan-2-yl)tetradecahydro-6H-5,10-methanocyclopenta[a]phenanthren-3-yl pivaloate 5. Compound **4** (1.1128 g, 2.286 mmol) was dissolved in pyridine (11.43 mL). The reaction was cooled to 0°C and methanesulfonyl chloride (0.885 mL, 11.43 mmol) was added dropwise, and the reaction was stirred at 0°C for 2 hours. The reaction was then quenched with 20 mL of cold water, and extracted with dichloromethane 3 times. The organic layer was then washed with brine, and the solvent was removed in vacuo. The resulting residue was resuspended in 3-pentanone (76 mL), and a solution of potassium acetate (1.2339 g in 23 mL water) was added. The reaction was then stirred at 120°C for 48 hours. When TLC indicated the consumption of starting material, the reaction was allowed

to cool to room temperature, and extracted with ethyl acetate. The material was loaded onto Florosil gel, and purified by flash chromatography (20 g silica, 1:19 EtOAc:Hexane) to give **5** as a white solid (0.5677, 51%). **TLC** R_F = 0.34, 1:4 EtOAc:Hexane. **^{1}H-NMR** (400.53 MHz, $CDCl_3$): δ 4.74-4.66 (1H, m, 3α-H), 4.10 (1H, bs), 2.16-2.11 (1H, m), 2.06-1.98 (2H), 1.91-1.68 (5H), 1.57-1.43 (4H), 1.37-1.25 (3H), 1.22-1.18 (3H), 1.16 (9H, s, 3β-OPiv), 1.13-0.99 (9H), 0.91-0.85 (10H), 0.65 (3H, s), 0.31 (1H, d, J = 4.9 Hz). **^{13}C-NMR** (100.13 MHz, $CDCl_3$): δ 178.06, 73.92, 70.05, 56.38, 54.64, 48.19, 43.03, 39.96, 39.86, 39.48, 38.62, 37.24, 36.12, 35.72, 29.38, 28.18, 28.00, 27.46, 27.13, 26.66, 26.10, 25.11, 23.91, 23.81, 22..81, 22.55, 18.65, 15.59, 12.25. **HR-MS** (ESI+) $[M+Na]^+$ Calculated for $C_{32}H_{54}O_3$: 509.3965; Found: 509.3969. $[2M+Na]^+$ Calculated for $C_{64}H_{108}O_6$: 995.8038; Found 995.8049.

(3S,6R,13R,17R)-13-methyl-17-((R)-6-methylheptan-2-yl)-6-(((methylsulfonyl)oxy)methyl)-2,3,4,6,7,8,9,11,12,13,14,15,16,17-tetradecahydro-1H-cyclopenta[a]phenanthren-3-yl pivaloate (6-Methyl(methanesulfonyl)-19-norcholest-5(10)-en-3-yl pivaloate) 6. Compound **5** (0.4000 g, 0.82 mmol) was dissolved in dichloromethane (8 mL) under argon. Methanesulfonic acid (0.16 mL, 2.46 mmol) was added while stirring. The reaction mixture was cooled to 0°C, and boron trifluoride diethyl etherate (0.20 mL, 1.64 mmol) was added, and the reaction was stirred for 4 hours. The reaction was then extracted with dichloromethane, and washed with saturated sodium bicarbonate solution and brine. The combined aqueous layer was then extracted with diethyl ether 3 times. The combined organic layers were then dried over sodium sulfate, the material was loaded onto Florosil gel, and purified by flash chromatography (20 g Florosil, 1:9 EtOAc:Hexane) to give **6** as a clear residue (0.1607 g, 34.6%). **TLC** R_F = 0.29, 1:4 EtOAc:Hexane). **^{1}H-NMR** (400.53 MHz, $CDCl_3$): δ 4.94 (1H, m, 3α-H), 4.18 (1H, m, 6β-CH_2), 4.07 (1H, t, J = 9.79 Hz, 6β-CH_2), 2.98 (3H, t, J = 6.71 Hz, 6β-OMs). **^{13}C-NMR** (100.13 MHz, $CDCl_3$): δ 178.09, 135.67, 121.61, 70.66, 68.97, 56.29, 54.74, 46.48, 43.08, 40.12, 39.87, 39.47, 38.74, 37.43, 36.11, 35.74, 34.64, 33.68, 28.55, 28.27, 27.98, 27.14, 25.64, 24.42, 23.78, 23.60, 22.81, 22.55, 18.62, 12.27. **HR-MS** $[M+NH_4]^+$ Calculated for $C_{33}H_{56}O_5S$: 582.4187; Found 582.4196.

2. Radiochemistry

2.1. General Considerations.

Unless otherwise stated, reagents and solvents were commercially available and used without further purification:. Ethanol (200 proof, USP) was purchased from Decon Laboratories, Inc. Sodium chloride 0.9%, USP was sourced from Hospira. Other synthesis components were obtained as follows: Sterile vials were obtained from Hollister-Stier; QMA-light cartridges were purchased from Waters. Prior to use QMA cartridges were conditioned with ethanol (10

mL), 0.5 M $NaHCO_3$ (10 mL) and sterile water (10 mL). Acetonitrile was purchased from Alfa Aesar.

2.2. Procedure for Radiochemical Synthesis of [^{18}F]FNP-59

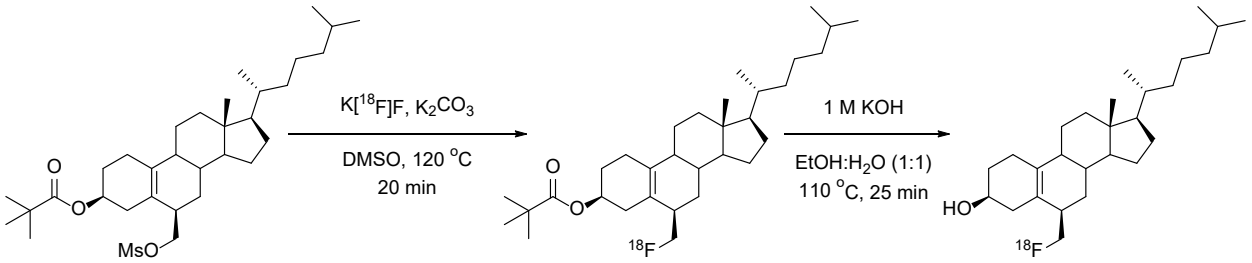

Figure S3: Radiosynthesis of [^{18}F]FNP-59.

Procedure for [^{18}F]FNP-59

The synthesis of [^{18}F]FNP-59 was accomplished using a General Electric (GE) TRACERLab $FX_{N\text{-}Pro}$ synthesis module loaded as follows: Vial 1: 500 µL of 7 mg/mL potassium carbonate in water; Vial 2: 1000 µL of ethanol and 15 mg of Krypotfix 2.2.2. Vial 3: 5 mg precursor in 1000 µL DMSO; Vial 4: 1000 µL of a 1M potassium hydroxide solution in H_2O:Ethanol (1:1). [^{18}F]Fluoride was produced via the $^{18}O(p,n)^{18}F$ nuclear reaction with a GE PETtrace cyclotron equipped with a high-yield fluorine-18 target. [^{18}F]Fluoride was delivered in a bolus of [^{18}O]H_2O to the synthesis module and trapped on a QMA-Light sep-pak cartridge to remove [^{18}O]H_2O. [^{18}F]Fluoride was then eluted into the reaction vessel with potassium carbonate (3.5 mg in 500 µL of water). Ethanol (1 mL) with 15 mg of Kyrptofix 2.2.2 was added to the reaction vessel, and the [^{18}F]fluoride was azeotropically dried by heating the reaction vessel to 100 °C and drawing full vacuum. After this time, the reaction vessel was subjected to both an argon stream and a simultaneous vacuum draw at 100 °C. The solution of precursor in DMSO (5 mg in 1000 µL) was added to the dried [^{18}F]fluoride, and as shown in figure 2 was heated at 120 °C with stirring for 20 min. Subsequently, the reaction mixture was cooled to 50 °C, and the 1M potassium hydroxide solution was added. The reaction mixture was heated at 110 °C for 25 minutes. The reaction mixture was cooled and HPLC eluent (80% Ethanol: 20% H_2O, 3 mL) was added. The material was injected onto a Phenomenex Luna C18(2) 250x10 mm, 10 µ column and eluted at 5 mL/min. The product peak was collected into reactor two of the Tracerlab module. The collected [^{18}F]FNP-59 was azeotropically dried by heating the reaction vessel to 100 °C and drawing full vacuum. After this time, the reaction vessel was subjected to both an argon stream and a simultaneous vacuum draw at 100 °C. [^{18}F]FNP-59 was then dissolved in an ethanol (0.66 mL) Tween® 80 (polysorbate; 0.16 mL) solution. After [^{18}F]FNP-59 was dissolved, the solution was diluted with saline (9.18 mL). The solution was passed through a sterile filter and a sample was removed for quality control.

2.3. FNP-59 Manufacturing Flow Diagram

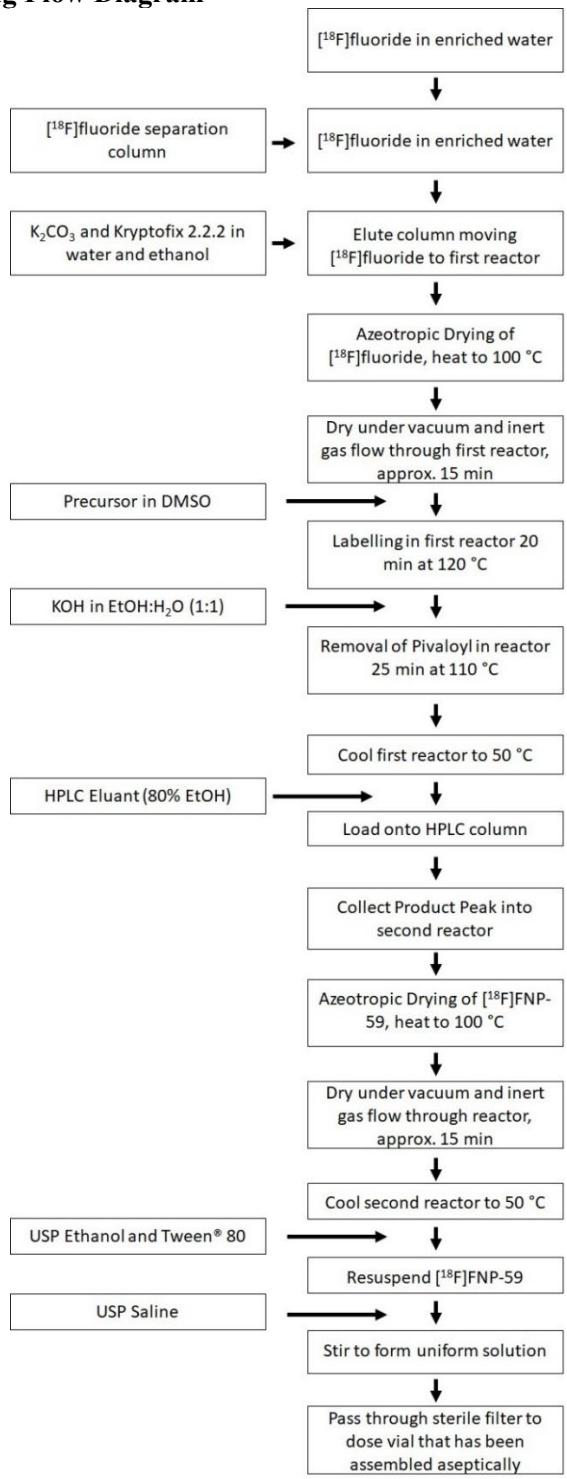

2.4. Representative Batch Data

Representative production scale batches with complete QC testing were produced to verify the consistency of the manufacturing process and are summarized below. These batches met the established release criteria for each of the quality control tests. No pooling or averaging of results was used to obtain passing results.

Batch Data	**021020FNP59-01**	**021120FN59-02**	**021320FNP59-03**	**Mean Results**
Final formulated Volume (mL)	9.1	9	9	9.0
Total Radioactivity EOS (mCi)	22.8	57.1	52.5	44.1
Total FNP-59 Mass	<0.01 mg/mL	<0.01 mg/mL	<0.01 mg/mL	<0.01 mg/mL
Strength (mCi/mL)	2.51	6.34	5.83	4.89
Radiochemical Purity (%)	98.03	100	99.16	99.06
Kryptofix Analysis	<50 ug/mL	<50 ug/mL	<50 ug/mL	<50 ug/mL
Radionuclide Identity (half-life; min)	109.15	113.11	113.01	111.76
Radiochemical Identity	1.046	0.988	1.007	1.01
pH	6	6	7	6.3
Bacterial Endotoxins (EU/mL)	<2.00	<2.00	<2.00	<2.00
Visual Inspection	Pass	Pass	Pass	Pass
Filter membrane Integrity test	47	46	47	47
Sterility	Pass	Pass	Pass	Pass

2.5. Radio-HPLC and Radio-TLC Evaluation of [^{18}F]FNP-59

Evaluation of significant chemical species in each batch is performed using the HPLC or TLC system outlined below. Fluorination with ^{18}F during the preparation results in the substitution of the precursor methanesulfonate with fluoride to produce [^{18}F]FNP-59. The semi-preparative HPLC will isolate [^{18}F]FNP-59 from precursor and reaction side products. The total amount of [^{18}F]FNP-59 will be less than 0.01 mg/mL of dose (100 µg per batch). The content of [^{18}F]FNP-59 as detectable in each batch was determined prior to release.

HPLC Conditions

Column:	Phenomenex Luna C18(2) 150x4.6 mm, 3µ
Eluent:	80 % Ethanol, 20 % H_2O
Flow Rate:	0.75 mL/min
Detection:	Evaporative light scattering detector (ELSD), Ultra-Violet detector at 212 nm, Eckert & Ziegler HPLC gamma for detection of radioisotopes

TLC Conditions

Column:	75mm silica gel TLC plate with a baseline at 10mm
Eluent:	1:3 ratio mixture of Ethyl Acetate:Hexanes
Detectors:	Eckert & Ziegler TLC-Scanner for detection of radioisotopes; Iodine Stain Test

Semi-Preparatory Isolation of [^{18}F]FNP-59

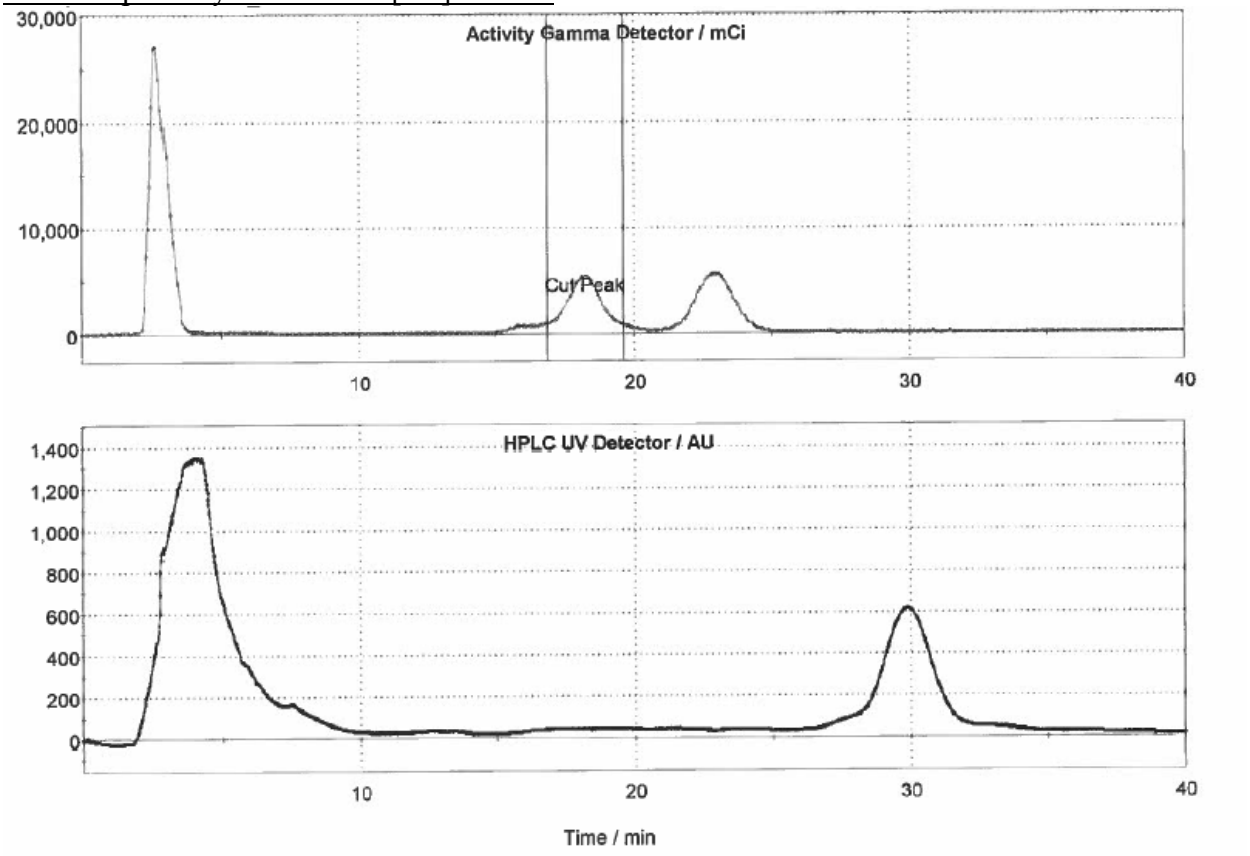

HPLC of Precursor

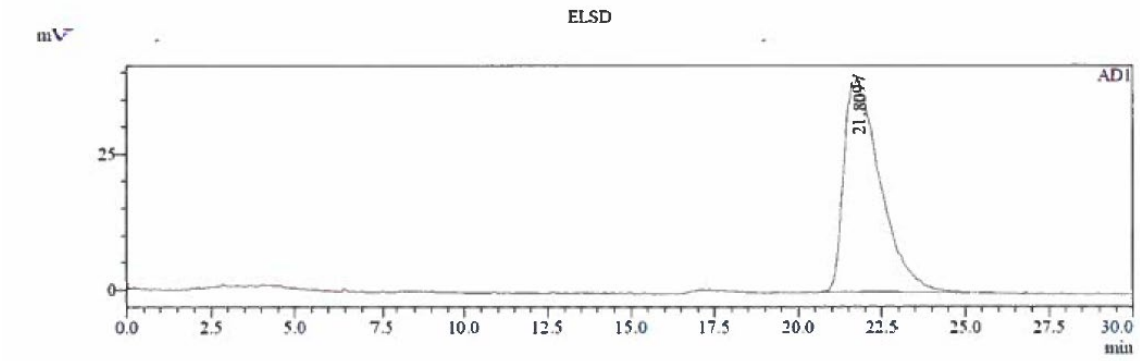

Peak Table Test quick batch_622020_001 lcd

AD1

Peak#	Name	Ret. Time	Area	Area%	Height	S/N	Resolution(USP)
1		21.809	2976006	100.000	39574	212.11	--
Total			2976006	100.000	39574		

Precursor detected using ELSD due to the lack of a significant chromophore for UV detection.

HPLC Reference Standard

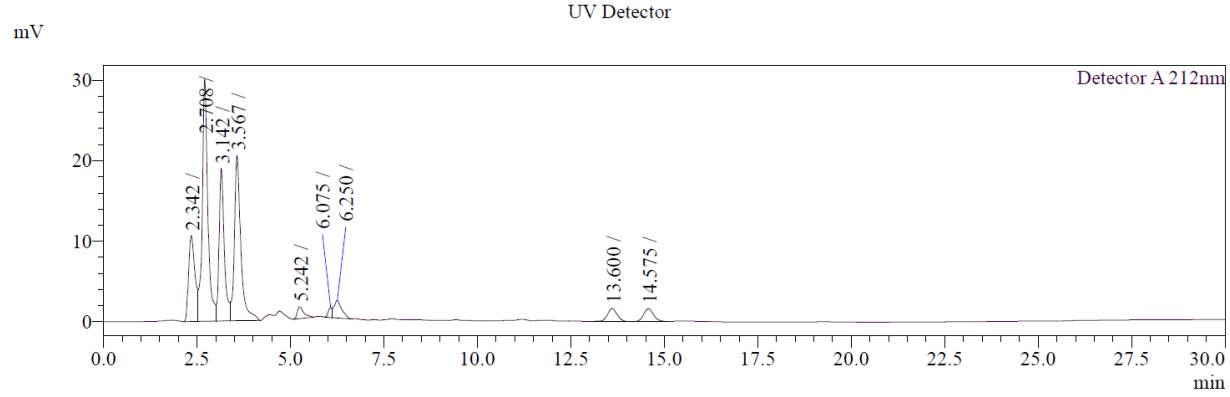

Reference Standard elutes as a broad signal with two peaks from ~13.6-14.6, with the same peak shape observed with cholesterol in HPLC system.

Formulation Solution

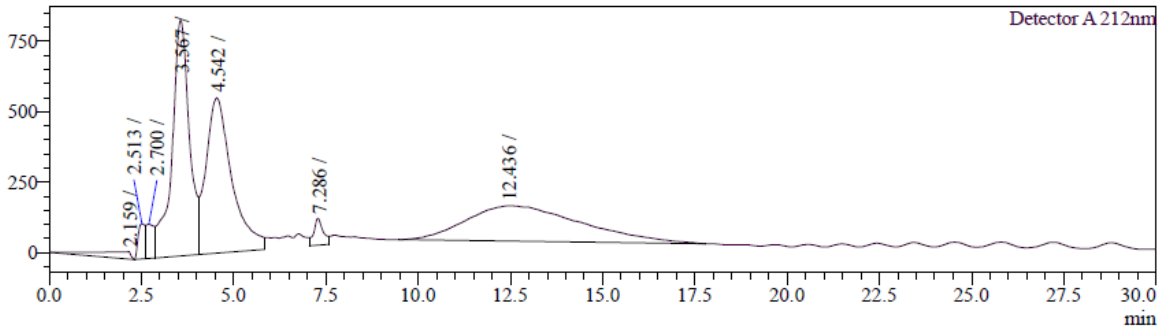

Broad peak from Tween® 80 observed at ~10-16 min and peaks in early potion of spectra <5 min due to ethanol and solution components due to use of 212 nm wavelength utilized.

Dose in Formulated Solution

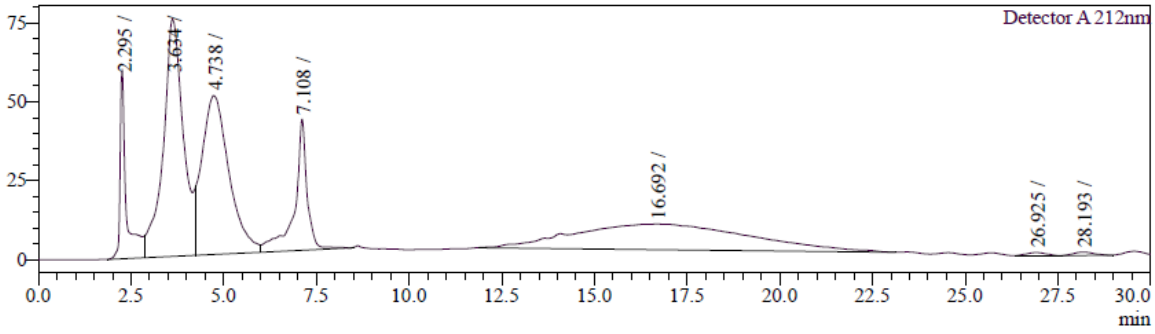

Tween® 80 signal is observed as well as formulation components and FNP-59 is below limit of quantification.

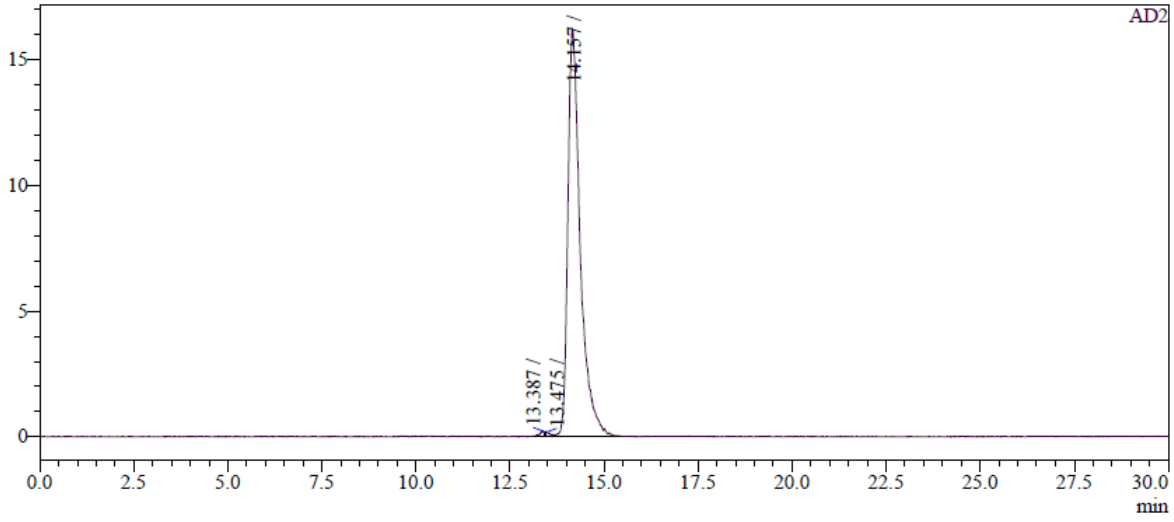

Peak Table

AD2

Peak#	Name	Ret. Time	Area	Area%	Height	Resolution(USP)
1		13.387	1707	0.455	218	--
2		13.475	1430	0.382	177	0.111
3		14.157	371618	99.163	16279	0.707
Total			374754	100.000	16674	

Gamma detection shows one major signal at expected retention time.

Co-Injection

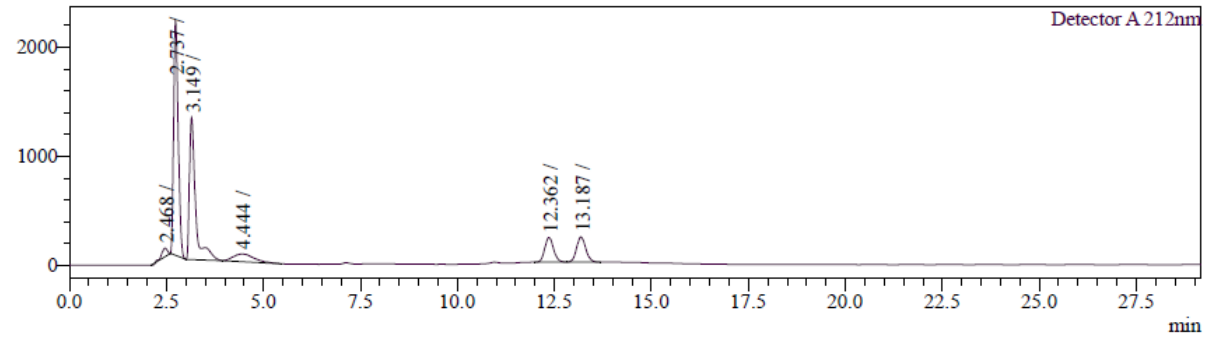

Standard signal clearly seen in UV.

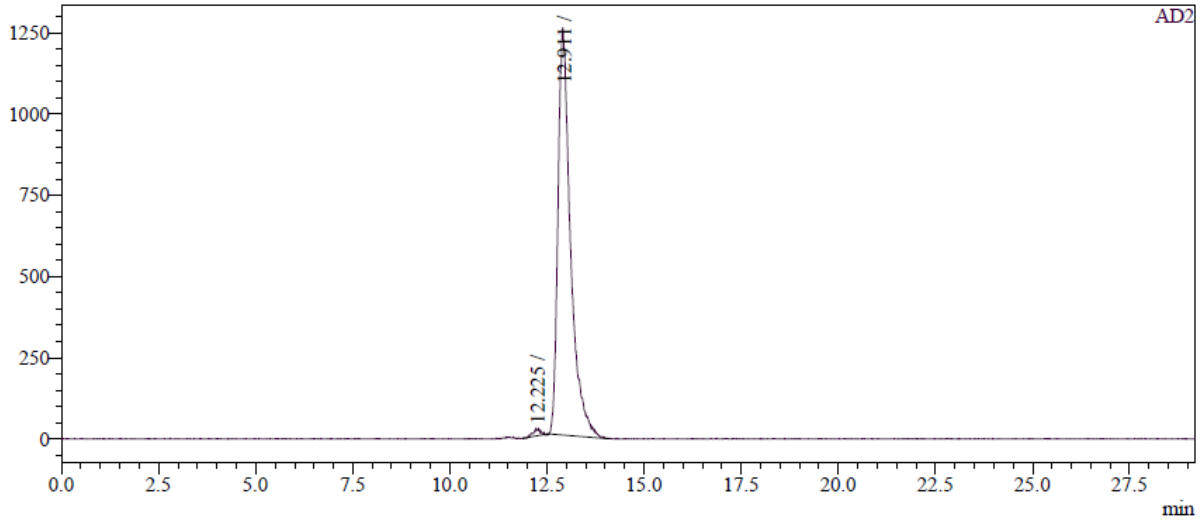

Gamma signal at time that correlates with center of broad double peaked signal observed in UV spectrum from injection.

4-Hr Stability Study

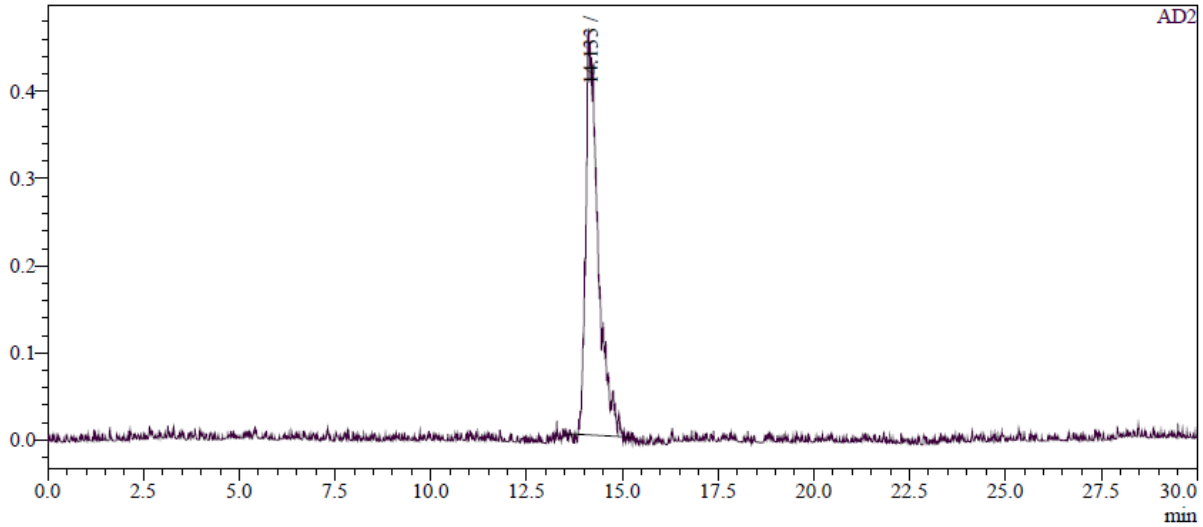

Freshly drawn sample from dose vial at 4 hr from end of synthesis shows a single gamma signal at the expected retention time.

TLC Analysis Data

Reg	(mm) Start	(mm) Stop	(mm) Centroid	RF	Region Counts	Region CPM	% of Total	% of ROI
Rgn 1	53.8	63.3	59.1	-0.013	1092.0	1092.0	1.79	1.80
Rgn 2	64.2	103.0	82.0	0.339	59536.0	59536.0	97.44	98.20
2 Peaks					60628.0	60628.0	99.22	100.00

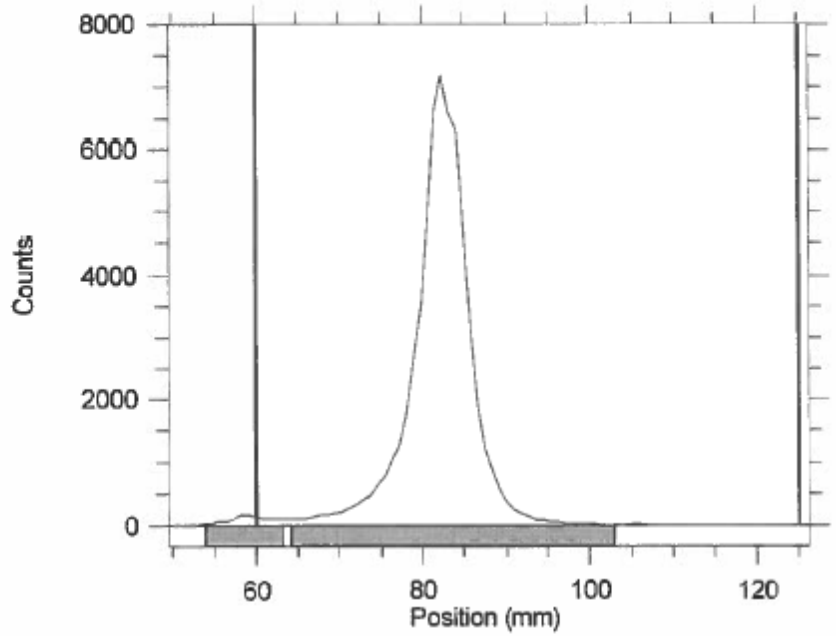

Single peak observed by radioTLC scanner

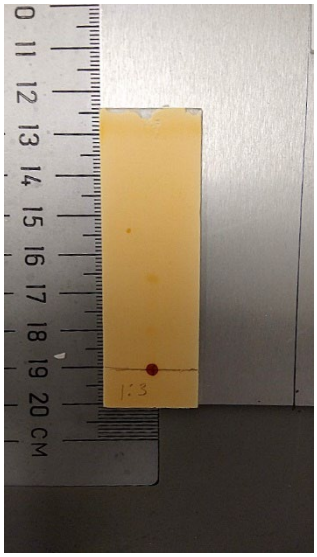

Iodine staining shows spot in expected R_f range around 0.34 and at baseline from buffer components of formulation.

3. Biodistribution and Radiation Dosimetry Study

3.1.Biodistribution Study

Biodistribution experiments were conducted at 10,30, 60, 120, and 360 min post-injection of [^{18}F]FNP-59. Briefly, male (n = 10) and female (n = 10) Sprague-Dawley rats (weighing 171 - 339 g) were anesthetized with isoflurane (5% induction, 1-2% maintenance), injected i.v. with [^{18}F]FNP-59 (3349 ± 827 kBq for 10 min; 3709 ± 255 kBq for 30 min; 3312 ± 608 kBq for 60 min; 3645 ± 71 kBq for 120 min; 8297 ± 237 kBq) via the lateral tail vein and allowed to awaken until sacrifice. 2 M and 2F rats were sacrificed at each time point (10, 30, 60, 120, and 3600 min post-injection). Tissues and organs were collected, weighed and counted for their radioactivity with a Packard 5550 autogamma counter. Results were averaged for each time point and expressed as % injected dose/gram of tissue for each organ (Table S1 and Figure S1). Less organs were analyzed at 360 minutes as focus was on organs that had yet to plateau in uptake at 120 minutes to get more accurate estimates of uptake and dosimetry.

	10 min			30 min			60 min			120 min			360 min		
	%ID/g Mean ± SD			%ID/g Mean ± SD			%ID/g Mean ± SD			%ID/g Mean ± SD			%ID/g Mean ± SD		
BRAIN	0.0641	±	0.0083	0.0466	±	0.0219	0.0540	±	0.0091	0.0487	±	0.0096	-	-	-
EYEBALLS	0.0449	±	0.0096	0.0309	±	0.0166	0.0490	±	0.0216	0.0507	±	0.0157	-	-	-
HEART	0.3757	±	0.1099	0.3328	±	0.1278	0.4235	±	0.0504	0.4598	±	0.0681	0.3926	±	0.1240
LUNG	1.2275	±	0.0640	1.2106	±	0.5238	1.4888	±	0.2530	1.4494	±	0.3417	0.9457	±	0.2393
LIVER	1.5336	±	0.4145	1.6659	±	0.5409	1.9378	±	0.3823	1.7309	±	0.1343	0.9934	±	0.2447
PANCREAS	0.1868	±	0.0258	0.1518	±	0.0490	0.2167	±	0.0387	0.2279	±	0.0314	-	-	-
SPLEEN	1.2604	±	0.1476	1.4934	±	0.5636	2.2259	±	0.4597	2.2159	±	0.5608	1.3867	±	0.4161
ADRENAL	1.7071	±	0.5681	1.7439	±	0.9175	2.8827	±	1.0246	3.6480	±	1.6686	7.3932	±	4.7215
KIDNEY	0.1993	±	0.0711	0.2567	±	0.1083	0.3350	±	0.0324	0.3559	±	0.0704	0.3201	±	0.1220
ADIPOSE	0.0601	±	0.0157	0.0756	±	0.0541	0.0996	±	0.0431	0.1006	±	0.0050	-	-	-
STOMACH	0.1865	±	0.1000	0.1232	±	0.0471	0.1647	±	0.0276	0.1621	±	0.0285	-	-	-
CONTENTS OF STOMACH	0.0042	±	0.0044	0.0123	±	0.0088	0.0208	±	0.0315	0.0083	±	0.0073	-	-	-
SMALL INTESTINE	0.2219	±	0.0252	0.4025	±	0.1087	0.6010	±	0.1517	0.8053	±	0.1736	0.4762	±	0.1707
CONTENTS OF SMALL INTESTINE	0.0110	±	0.0178	0.3316	±	0.2129	0.5314	±	0.2189	0.8329	±	0.1987	-	-	-
CAECUM	0.0856	±	0.0055	0.0951	±	0.0446	0.1400	±	0.0333	0.1248	±	0.0380	-	-	-
CONTENTS OF CAECUM	0.0009	±	0.0007	0.0020	±	0.0023	0.0026	±	0.0020	0.0038	±	0.0040	-	-	-
LARGE INTESTINE	0.0795	±	0.0085	0.0799	±	0.0252	0.2196	±	0.2358	0.1495	±	0.0540	-	-	-
CONTENTS OF LARGE INTESTIN	0.0010	±	0.0010	0.0081	±	0.0140	0.0515	±	0.1000	0.2321	±	0.3344	-	-	-
OVARY	0.7330	±	0.1401	0.6571	±	0.1551	1.0159	±	0.4046	1.3124	±	0.6178	2.6982	±	2.1813
UTERUS	0.1327	±	0.0097	0.1686	±	0.0352	0.1902	±	0.0154	0.2609	±	0.0479	-	-	-
MUSCLE	0.0521	±	0.0056	0.0635	±	0.0263	0.0927	±	0.0152	0.0976	±	0.0177	-	-	-
BONE	0.1488	±	0.0395	0.1485	±	0.0487	0.2382	±	0.0306	0.2741	±	0.0616	-	-	-
BLOOD	1.2156	±	0.1111	0.9028	±	0.3768	0.9339	±	0.1644	0.7371	±	0.1791	0.3864	±	0.1243
TESTES	0.0188	±	0.0024	0.0146	±	0.0076	0.0365	±	0.0085	0.0381	±	0.0088	0.0370	±	0.0022

3.2. Human Radiation Dosimetry Estimates

Biodistribution studies were conducted in male and female Sprague Dawley rats as described above. Biodistribution data was used to determine radiation-absorbed-dose estimates using the OLINDA/EXM 2.0 software package.[2,3] Distribution to the urine was also determined by acquiring dynamic small animal PET scans from 0-120 min for male (n=2) and female (n=2) with bladder in frame, which showed no accumulation in the urine and allowed for calculation of radiation dose from above data.

^{18}F-NP59	Gender Averaged Dose (mSv/MBq)	Gender Averaged Dose (rem/mCi)
Target Organ		
Adrenals	6.82E-02	2.53E-01
Brain	3.70E-03	1.37E-02
Breasts	1.17E-02	4.31E-02
Esophagus	1.43E-02	5.27E-02
Eyes	5.22E-03	1.94E-02
Gallbladder Wall	2.11E-02	7.80E-02
Left colon	2.85E-02	1.06E-01
Small Intestine	5.14E-02	1.90E-01
Stomach Wall	1.57E-02	5.82E-02
Right colon	5.76E-02	2.13E-01
Rectum	1.65E-02	6.08E-02
Heart Wall	1.60E-02	5.92E-02
Kidneys	1.51E-02	5.57E-02
Liver	3.45E-02	1.28E-01
Lungs	2.44E-02	9.03E-02
Ovaries	3.11E-02	1.15E-01
Pancreas	1.68E-02	6.20E-02
Prostate	1.32E-02	4.87E-02
Salivary Glands	1.10E-02	4.05E-02
Red Marrow	1.22E-02	4.49E-02
Osteogenic Cells	1.04E-02	3.84E-02
Spleen	3.36E-02	1.24E-01
Testes	6.02E-03	2.23E-02
Thymus	1.40E-02	5.17E-02
Thyroid	1.25E-02	4.60E-02
Urinary Bladder Wall	1.32E-02	4.87E-02
Uterus	1.54E-02	5.68E-02
Total Body	1.36E-02	5.02E-02
Effective Dose:	1.92E-02	7.12E-02

4. Single Dose Acute Toxicity Study

4.1. General Considerations.

The study was conducted by the MSU In Vivo Facility in accordance with current guidelines for animal welfare (Guide for the Care and Use of Laboratory Animals, 8th Ed., 2011). The procedures used in this study have been reviewed and approved by the appropriate Institutional Animal Care and Use Committee.

4.2. Studies Conducted

The study was conducted in 10 male and 10 female Sprague Dawley Rats. The study included Clinical Observations, Food Consumption, Body Weight, Biochemistry, Complete Blood Counts, and Microscopic Evaluation of Tissues. The study concluded that FNP-59 (also known as 6-fluoromethyl-norcholesterol, FMNC) had a no-observed-adverse-effect-level (NOAEL) greater than 416 µg/Kg in Sprague Dawley rats. Data for study is contained in second supplemental document for publication.

5. References

(1) Winton WP, Brooks AF, Wong KK, Scott PJH, Viglianti BL. Synthesis of 6-(Fluoromethyl)-19-norcholest-5(10)-en-3-ol, a Fluorinated Analogue of NP-59, using the Mild Fluorinating Reagent, TBAF(Pinacol)(2). *Synopen* **2019**; 3(2): 55-8.

(2) Stabin, M. G.; Sparks, R. B.; Crowe, E. OLINDA/EXM: The Second-Generation Personal Computer Software for Internal Dose Assessment in Nuclear Medicine. *J. Nucl. Med.* **2005**, 46(6), 1023–1027.

(3) Stabin, M. G.; Siegel, J. A. Physical Models and Dose Factors for Use in Internal Dose Assessment. *Health Phys.* **2003**, 85(3), 294–310.

6. ^{1}H NMR, ^{13}C NMR and HRMS Spectra

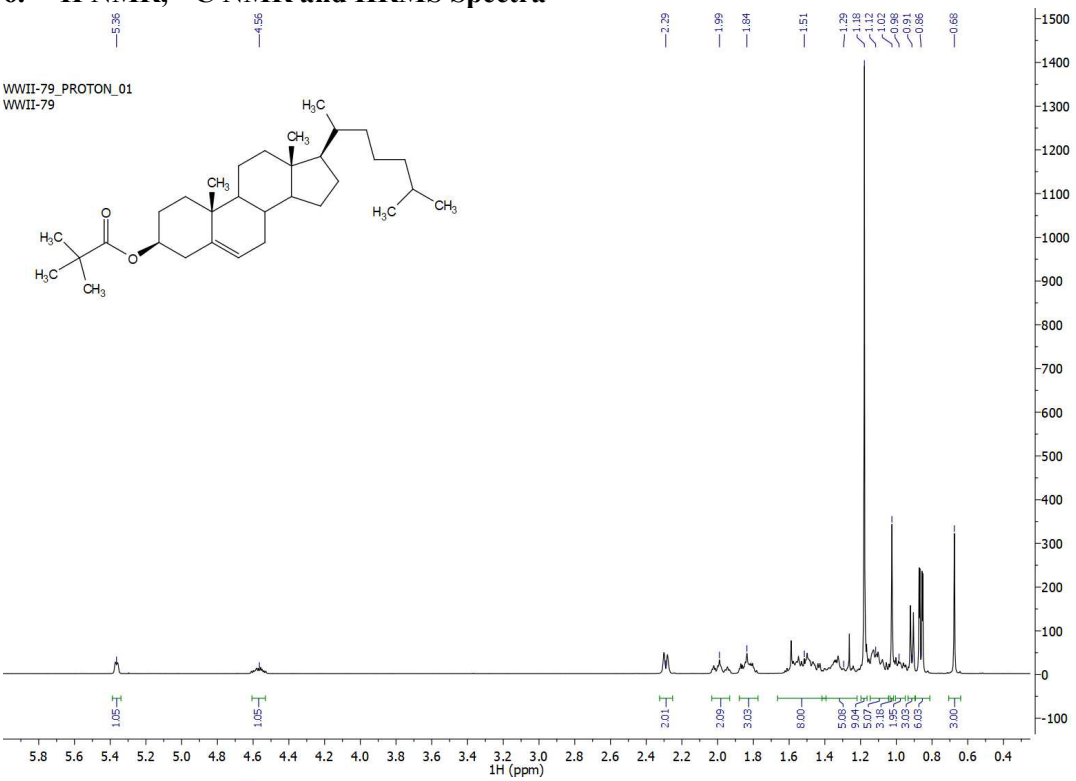

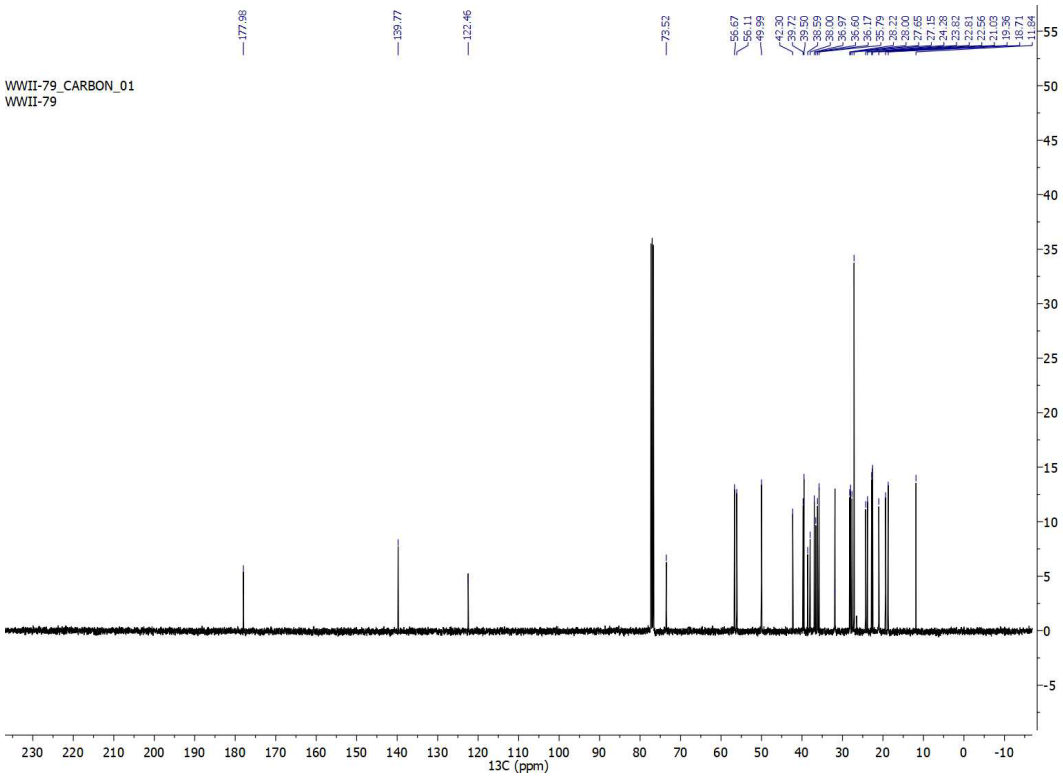

Wade Winton WW-II-79 ESI+

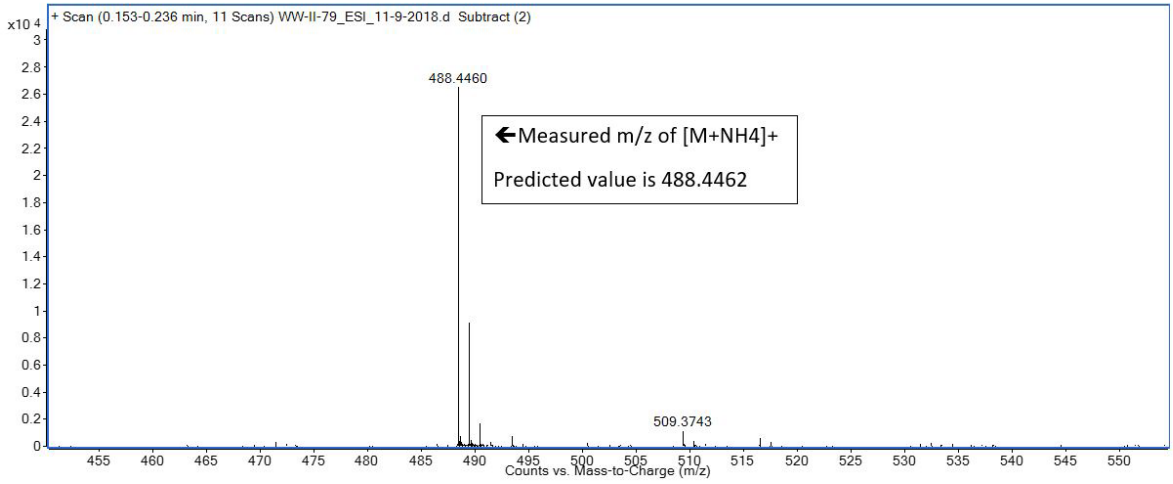

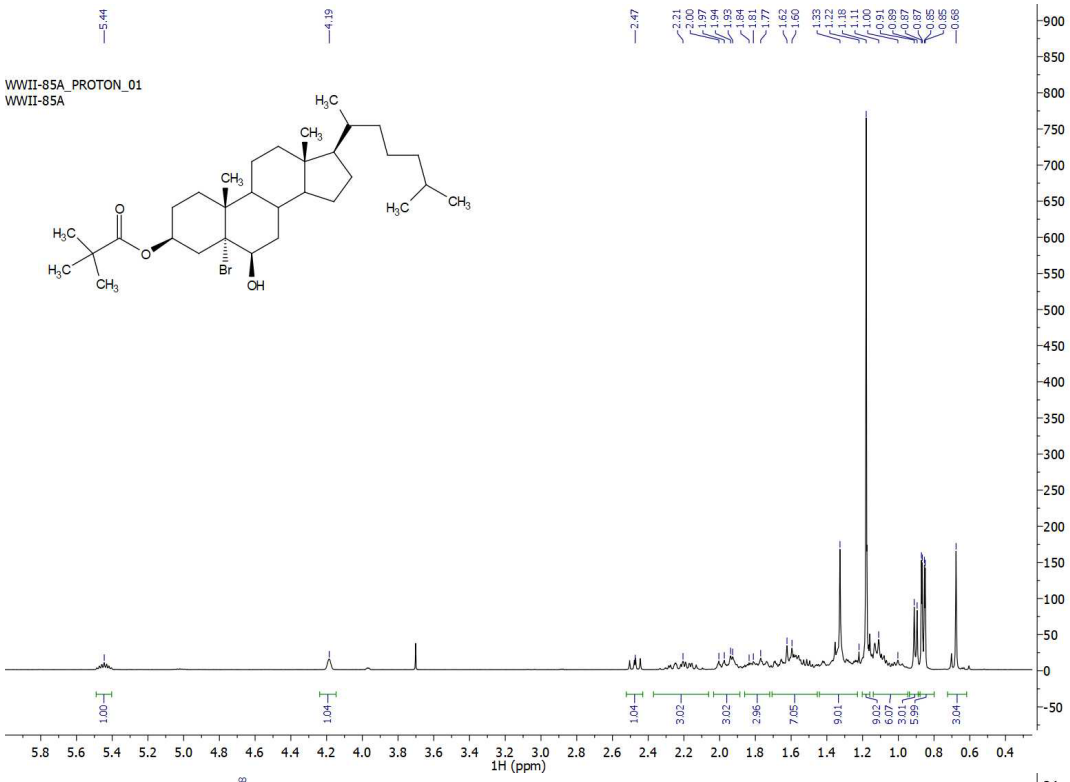
WWII-85A_PROTON_01
WWII-85A
5.44
4.19
2.47
2.21
2.00
1.97
1.94
1.93
1.84
1.81
1.77
1.62
1.60
1.33
1.22
1.18
1.11
1.00
0.91
0.89
0.87
0.87
0.85
0.85
0.68
1.00
1.04
1.04
3.02
3.02
2.96
7.05
9.01
9.02
6.07
3.01
5.99
3.04
1H (ppm)

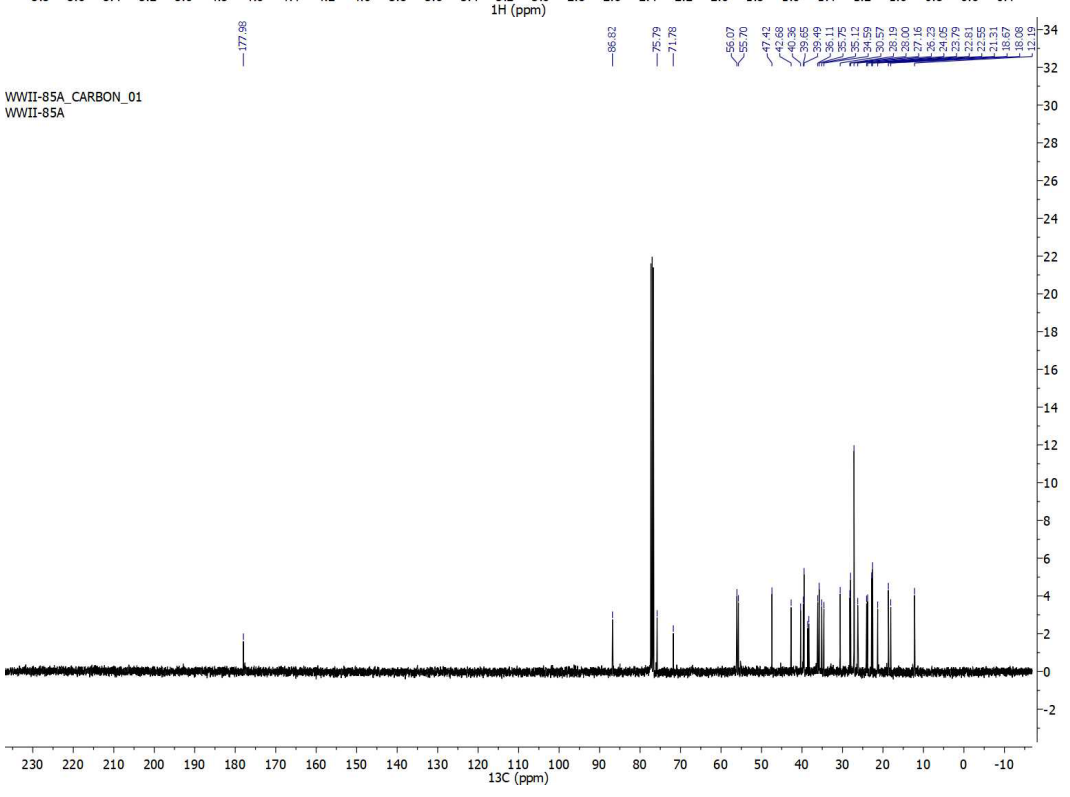
WWII-85A_CARBON_01
WWII-85A
177.98
86.82
75.79
71.78
56.07
55.70
47.42
42.68
42.36
39.65
39.49
36.11
35.75
35.12
34.59
30.57
28.19
28.00
26.16
26.23
24.05
23.79
22.81
22.55
21.31
18.67
18.08
12.19
13C (ppm)

Wade Winton WW-II-85-A ESI+

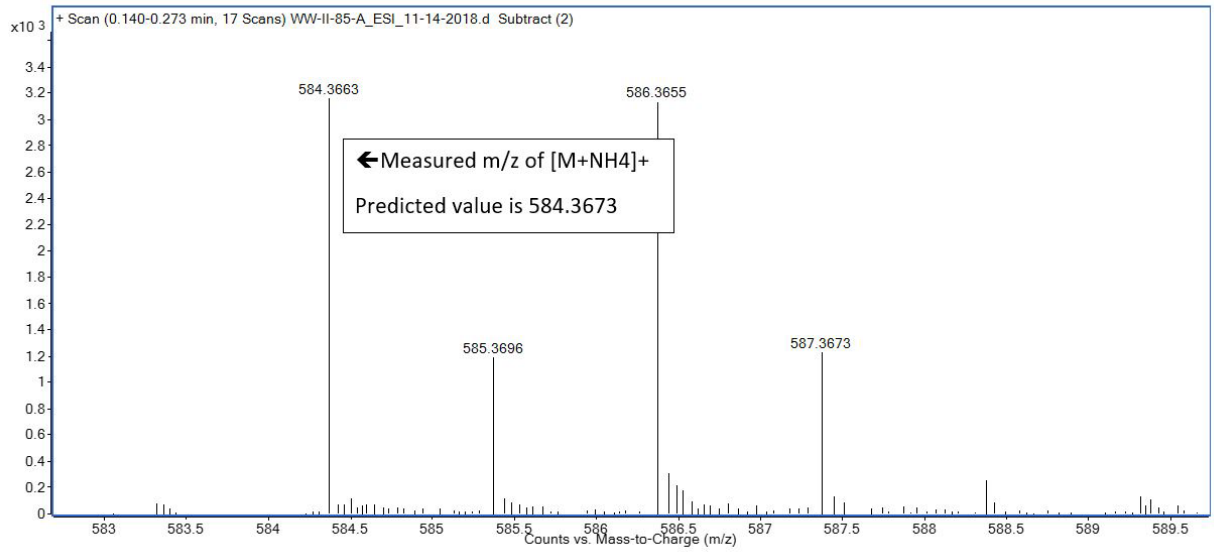

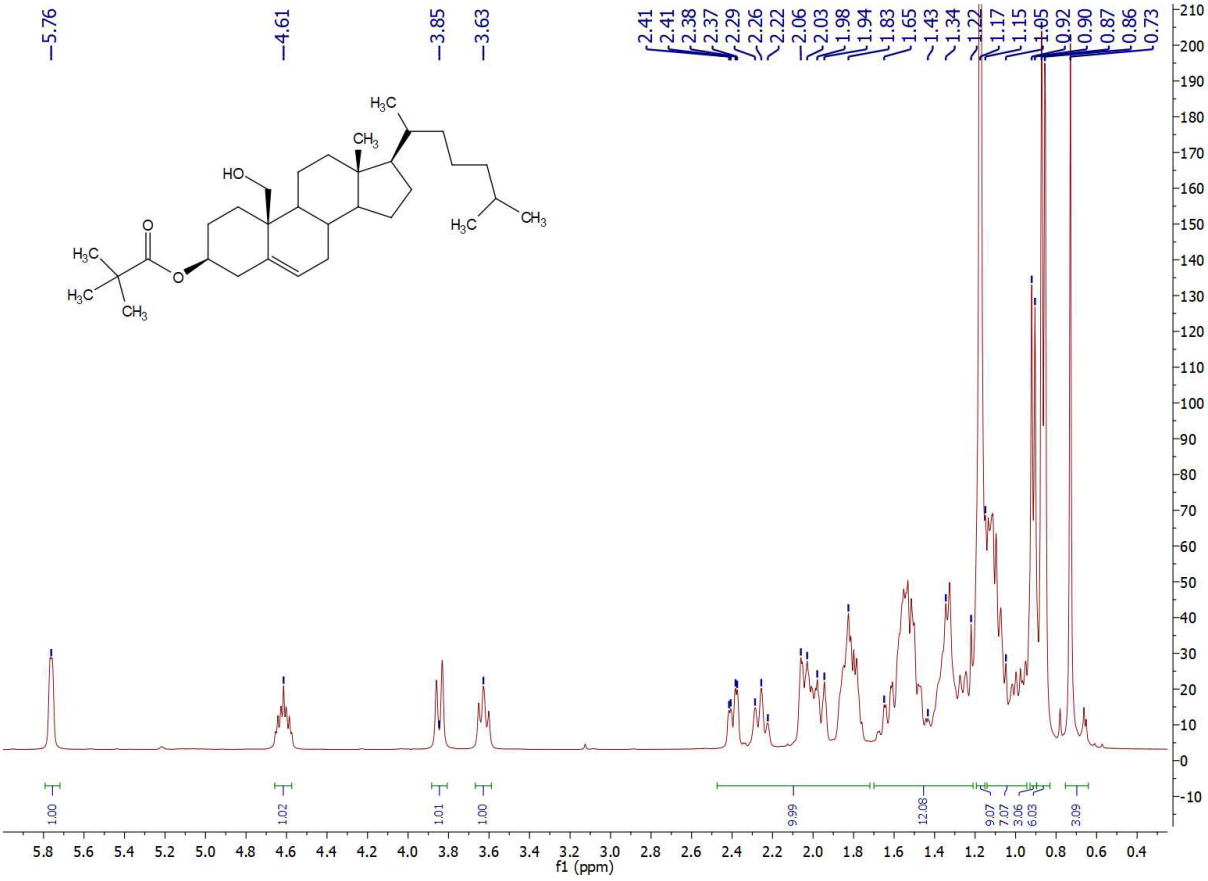

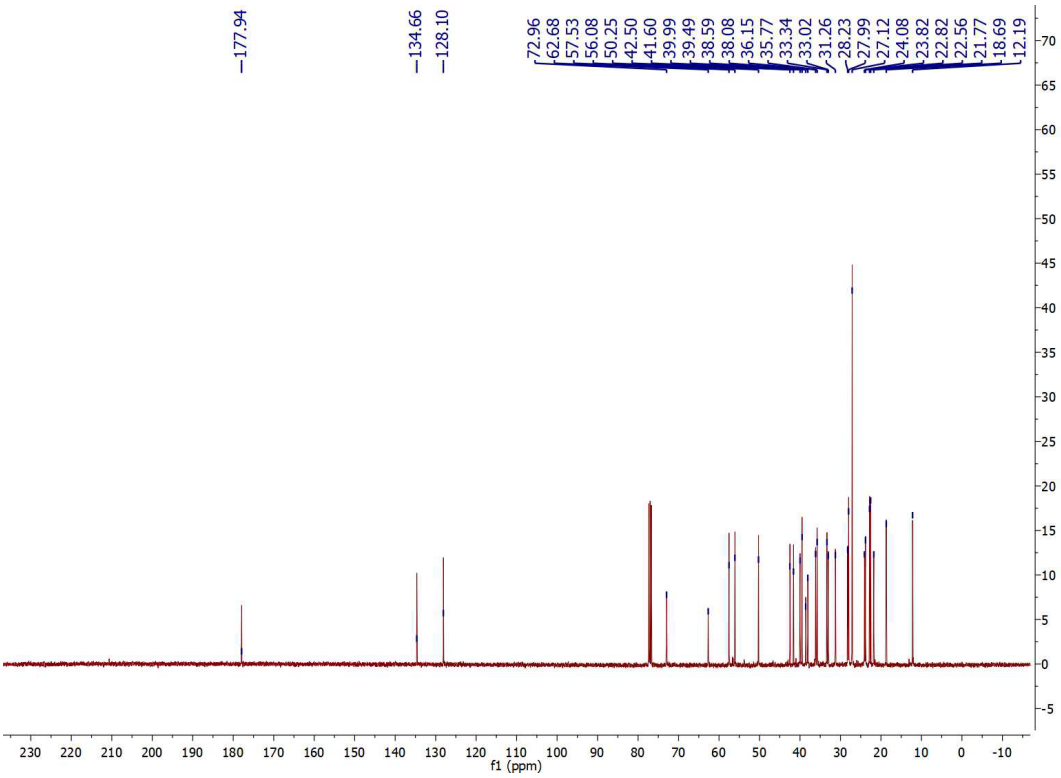

Wade Winton AFB-X-99 ESI+

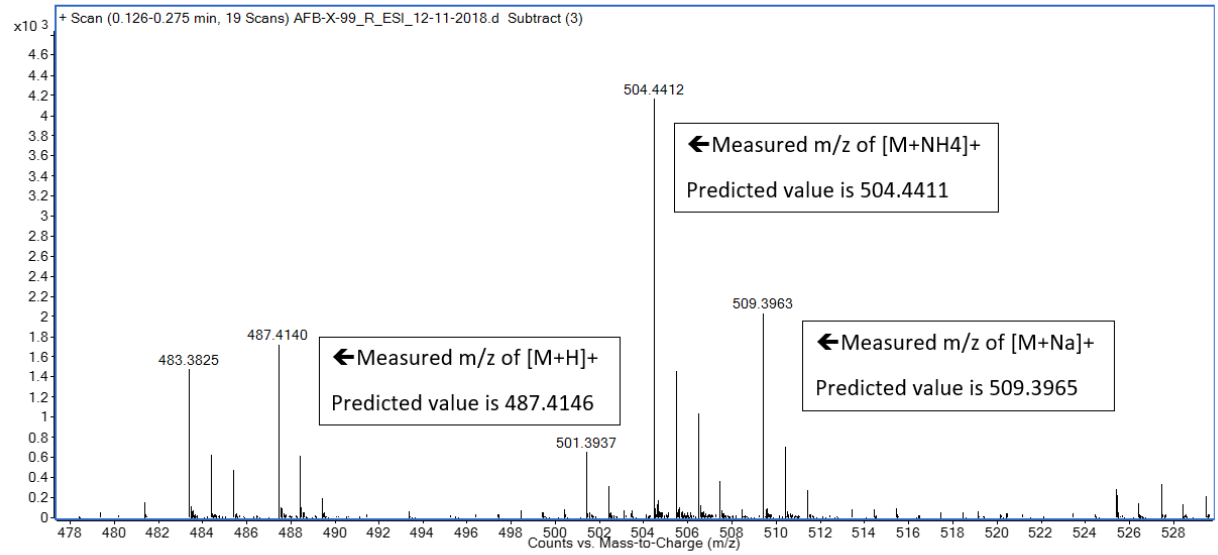

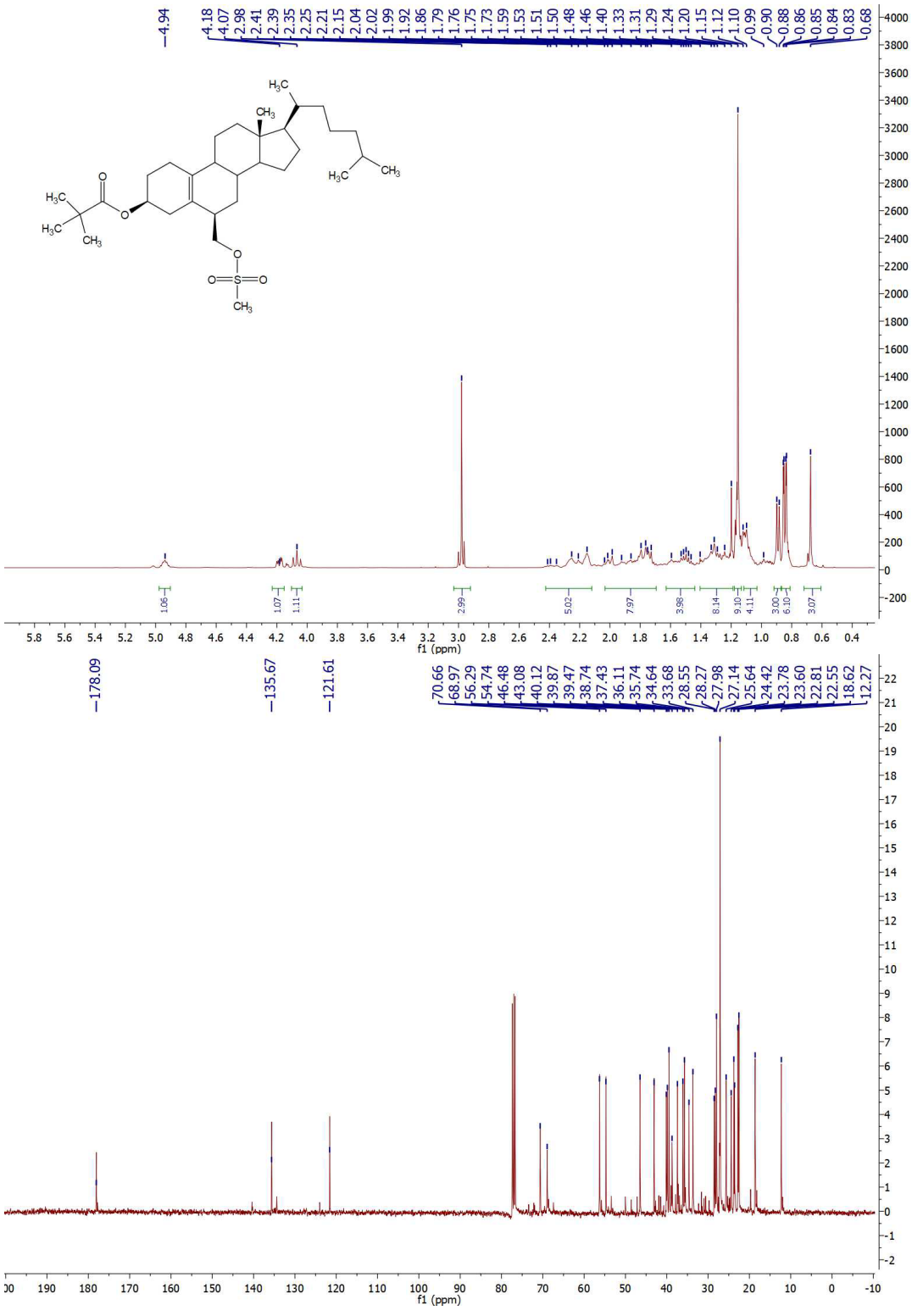
4.94
4.18
4.07
2.98
2.41
2.39
2.35
2.25
2.21
2.15
2.04
2.02
1.99
1.92
1.86
1.79
1.76
1.75
1.73
1.59
1.53
1.51
1.50
1.48
1.46
1.40
1.33
1.31
1.29
1.24
1.20
1.15
1.12
1.10
0.99
0.90
0.88
0.86
0.85
0.84
0.83
0.68
1.06
1.07
1.11
2.99
5.02
7.97
3.98
8.14
9.10
4.11
3.00
6.10
3.07
f1 (ppm)
178.09
135.67
121.61
70.66
68.97
56.29
54.74
46.48
43.08
40.12
39.87
39.47
38.74
37.43
36.11
35.74
34.64
33.68
28.55
28.27
27.98
27.14
25.64
24.42
23.78
23.60
22.81
22.55
18.62
12.27
f1 (ppm)

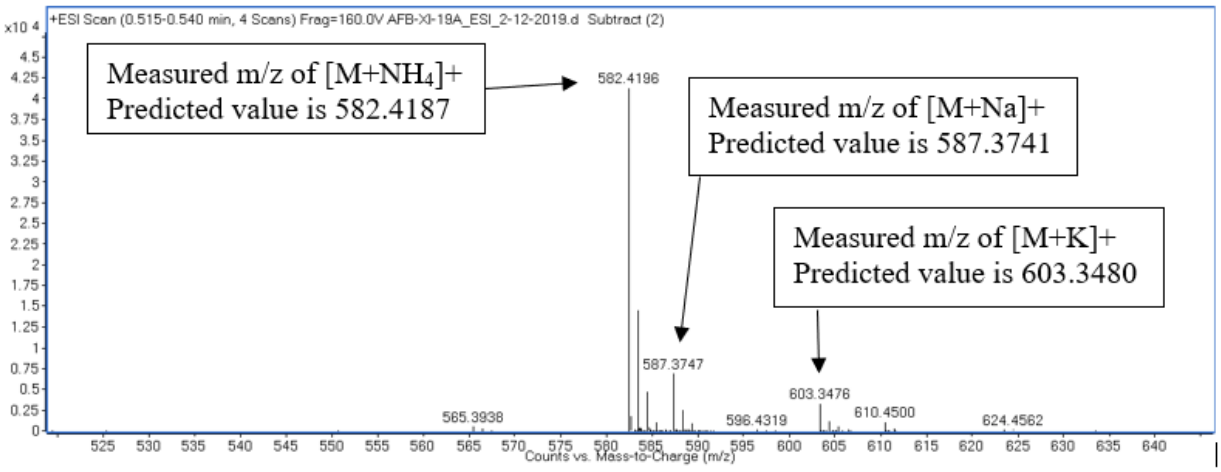
+ESI Scan (0.515-0.540 min, 4 Scans) Frag=160.0V AFB-XI-19A_ESI_2-12-2019.d Subtract (2)
x10 4
Measured m/z of [M+NH4]+
Predicted value is 582.4187
582.4196
Measured m/z of [M+Na]+
Predicted value is 587.3741
Measured m/z of [M+K]+
Predicted value is 603.3480
587.3747
603.3478
610.4500
565.3938
596.4319
624.4562
Counts vs. Mass-to-Charge (m/z)